Geochemical Clogging in Carbonate Mineralization on Carbon Dioxide Sequestration

Seung Youl Yoo

Abstract

Geological sequestration of carbon dioxide (CO_2) has been proposed as one of the most effective and advanced technologies for reducing CO_2 emissions. Geochemical trapping is regarded as one of the alternative process in CO_2 sequestration. Carbonate mineralization takes advantage of permeability reduction to seal formations with decreasing CO_2 leakage risk and increasing storage safety. As precipitation rates tend to be faster and the solubility product shows lower value at higher temperature, the calcite- and kaolinite- rich rock interacted with CO_2-water is expected to form the scale in geothermal reservoirs. Ca^{2+} released from rocks could be removed as carbonate minerals (e.g. $CaCO_3$) during CO_2 injection into aquifer rocks. However, the permeability of reservoirs is not clear when and where calcite deposits with the amount of precipitation. In order to predict the time and space of clogging with carbonates precipitation, flow experiments and numerical calculation of advection-reaction model have been performed under various conditions.

For the application in the field tests, supersaturated carbonate fluid were picked up from the three fields, Ogachi, Matsushiro and Namikata site. These representative fluids were used for laboratory scaled experiments in the wide range of temperature, pH and concentration of reactants. Growth rates of mineral generally show temperature- and pH- dependence on chemical kinetics. Therefore fluid temperatures at the Ogachi, Matsushiro and Namikata site varied with high, middle, room temperatures respectively. The usage of neutral pH was applied to the Ogachi and Matsushiro case and one of high pH corresponded to the Namikata case. Experimental results such as flow rate or

permeability change will play a vital role to develop and validate the numerical simulation about clogging phenomena.

Calculated flow rates based on the proposed geochemical clogging model were compared with the experimentally observed data to determine precipitation rates. Supersaturated fluid has an advantage of improving the filtration which means an ability of a particle capture to collect on the surface of porous media. When the ratio of filtration coefficient (λ) to pore fluid velocity (u) increases, the injectivity near the injection point tends to be significantly reduced by carbonate clogging. Meanwhile, precipitation of carbonate with low λ / u can be located as far away from the inlet as possible. Hence, the influent concentration and hydraulic gradient corresponding to λ and u respectively were taken as a dominant design parameters available to change each condition.

Sensitive analysis with a geochemical clogging model is able to provide the optimized injection parameters how to migrate deposited particles further from the inlet and storage as much as possible in the pore space without clogging. After results, there are two valuable findings related in temperature and pH. At high temperatures for instance in the cases of the Ogachi and Matsushiro, the effect of the influent concentration is more critical than fluid pressure change. In contrast, at relatively low temperatures and high pH such as the Namikata case, higher hydraulic gradients make advantage for the mineral trapping without clogging problems rather than higher concentrations. In other words, injection parameters such as concentration and fluid pressure should be designed by the temperature and pH conditions which affect the further growth rates of carbonate minerals.

Acknowledgements

Contents

List of Figures and Tables

CHAPTER 1   INTRODUCTION

1.1   Research background

Greenhouse gas (GHG) including carbon dioxide (CO_2) greatly affect the temperature of the Earth. Global warming caused by the increase in GHG has become a worldwide issues recently. Japan also would seek to reduce CO_2 emissions by 25% below 1990 levels by 2020. If the global energy demand still points to continue burning fossil fuels while avoiding the man-made climate change, then we have to keep the CO_2 emitted from power generation and industry. Carbon Capture and Storage (CCS) will play a decisive role as the only technology available to mitigate GHG emissions from large-scale fossil fuel usage in fuel transformation, power generation and industry. The first part of a two-stage process in CCS is capture of CO_2. The other process called CO_2 sequestration is piping the captured gas towards reservoirs and trapping CO_2 in the pore space of rock mass. The ETP BLUE Map scenario, which assessed strategies for reducing GHG emissions by 50% by 2050, revealed that if Carbon Capture and Storage (CCS) technologies are not available, the overall cost to achieve a 50% reduction in CO_2 emissions by 2050 will increase by 70% (IEA, 2008). Therefore, CCS is an essential part of the portfolio to limit global warming with the least-cost efforts so that 100 CCS projects by 2020 and over 3000 by 2050 are needed.

However, CO_2 sequestration has been in operation with limited options such as enhanced oil and gas recovery, enhanced coal beds methane recovery, depleted oil, gas reservoirs and deep saline aquifers. Hence a new approach on a case-by-case needs is worth spreading more CCS projects around the world, although in relatively small scale.

1

Supercritical CO_2 above the critical points (31.1ºC and 7.38MPa) is likely to be movable in the deep aquifers because the buoyancy works upward by the difference of the density between CO_2 and formation water. Thus, there is possibility of CO_2 leakage in a surface of discontinuity for example faults. This thesis aims to find out how to accelerate precipitation of mineral, particularly artificial carbonates, to alleviate the leakage risk and facilitate CO_2 storage, although in areas with no continuous cap rock.

The first issue is the geochemical reactions of carbonate minerals, mainly focusing on several experimental studies. Evaluation of CO_2 sequestration capacity in deep saline aquifers is complicated since a lot of trapping mechanisms work on different time scales (Bachu et al., 2007). Particularly geochemical reactions such as dissolution and precipitation will take long term for CO_2 fixation. Reactive transport simulation provided that from 5 to 25% of injected CO_2 mass may be sequestered by precipitation of secondary carbonates in 10,000 years (Audigane et al., 2006; Xu et al., 2006). The high temperature is favorable for immediate mineral carbonation to overcome the slow geochemical reactions and contribute to the storage safety. Carbonate-rich rock formations is commonly found as hydromagnesite at low temperature in the ultramafic region (RITE, 2008) and calcite at high temperature in Sumikawa geothermal fields, Akita, Japan. CO_2-saturated groundwater has reacted with reservoir rocks according to the following reaction to form a carbonate and kaolinite alteration:

$$CaAl_2Si_2O_8 \text{ (plagiocla se)} + H^+ + HCO_3^- + H_2O = \\ CaCO_3 \text{ (calcite)} + Al_2Si_2O_5(OH)_4 \text{ (kaolinite)} \tag{1.1}$$
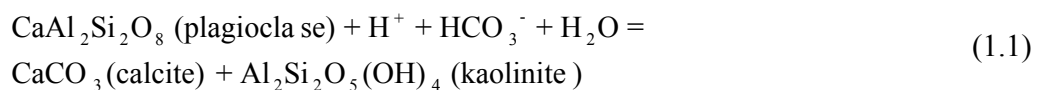
The chemical reaction moves towards the right side by decreasing solubility of calcite with higher temperature as shown in Fig. 1.1 (Chiba, 1991).

2
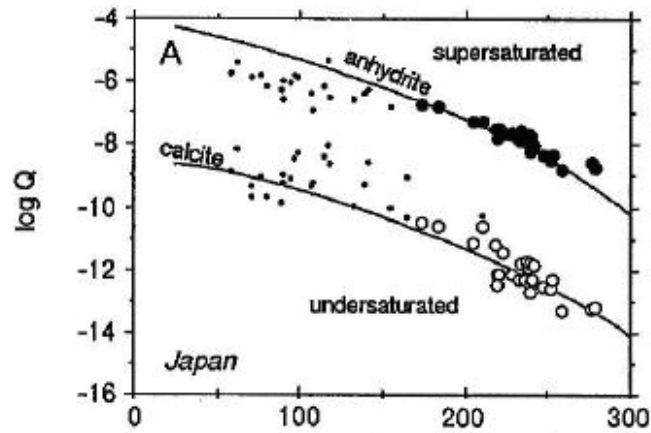
Fig. 1.1: Logarithm of activity product versus reservoir temperature: Open circles for
activity products of Ca^{2+} and CO_3^{2-} in geothermal fluid (after Chiba, 1991).

Experimental and theoretical investigations of reaction (1.1) have been reported
(Gales and Shane, 1905; Gunter and Bird, 1988). Precipitation kinetics of calcite have
been examined (Brown et al., 1993; Jonasson et al., 1996; Teng et al., 2000; Zhang and
Dawe, 2000) and fitted to second order expressions at elevated temperatures (Shiraki and
Brantley, 1995).

Field experiments have been conducted at the Ogachi Hot Dry Rock geothermal
site, Japan, in which water with dissolved CO_2 was injected into a high temperature
borehole (OGC-2, 210ºC) to study mineral trapping phenomena (Ueda et al., 2005;
Ozawa et al., 2006). The change of aqueous chemical evolution and groundwater level
provided undisputed evidence that mineral precipitation occurred. In order to reproduce
CO_2 sequestration into geothermal fields, results on CO_2-water-rock interaction showed
that calcite deposited from the alteration of plagioclase with reaction with CO_2 and Ca
from the rock at hydrothermal temperatures (Kuroda et al., 2009). In contrast with high
temperatures, the pilot-scale CO_2 injection test was performed under the relatively
moderate temperature environment at the Nagaoka site, where target formation is a
porous sandstone bed at a depth of 1100m. The injected CO_2 was in a supercritical state

3

since the temperature and pressure of formation water at the reservoir were 48 °C and 10.8 MPa respectively. Modelling results based on observed compositions of the formation water sampling after CO_2 injection implied that mineral trapping could occur from the early stage of CO_2 storage. Even if the temperature of formation fluid at Nagaoka site was not so high as one at Ogachi, the mineral precipitation can be far faster than one expected by IPCC (2005) (Mito et al., 2008).

The second issue is the filtration phenomenon of carbonate particles in advection-reaction equation. Carbonate mineralization takes advantage of permeability reduction to seal formations with a decreasing risk of CO_2 leakage while increasing storage safety. In spite of the benefit of self-sealing, fluid injectivity might decrease with time due to clogging reservoirs. Therefore, the determination of design parameters is the most important for CO_2 injection without clogging pore spaces while maximizing amount of fixed carbonates. However, there is little information about permeability changes by chemical reaction of CO_2 with reservoir rocks. Filtration is a key phenomenon to help explain the clogging mechanism by which fine mineral particles are transported through carbonate fluid and are extracted from solution by chemical reaction between fluid and rocks. The newly developed clogging model (Yoo et.al, 2011, 2012) suggests how to evaluate deposition rates and amount of carbonate precipitation by monitoring flow rates during CO_2 sequestration. Laboratory scale experiments and numerical simulations will exhibit insights for clogging phenomena of low permeable carbonate deposition with respect to location and time.

In this chapter, the previous researches on these subjects are reviewed, and the objectives and the outline of this dissertation are presented.

1.2   Research objectives and the outline

Experimental and numerical analysis on physico-chemical issues are presented. The aims of this research are shown in Fig. 1.2:

1) to clarify precipitation behaviors of carbonates by performing flow experiments at a laboratory scale and a field scale in the various range of temperatures and pH;

2) to develop a new step-wised numerical model applicable to flow experiments and predict permeability change with respect to location and time;

3) to evaluate precipitation rates and the amount of carbonates deposited in pore spaces;

4) to obtain the best conditions for mineral trapping how to migrate particles further from the inlet and storage as much as possible in the pore space without clogging.

Fig. 1.3 shows that the flow chart in this dissertation consists of six chapters. The outline of each chapter is described as follows:

In Chapter 1, the objectives and outline of this thesis are introduced.

In Chapter 2, the previous researches on mineralization and zero emission type of geothermal power plants are reviewed.
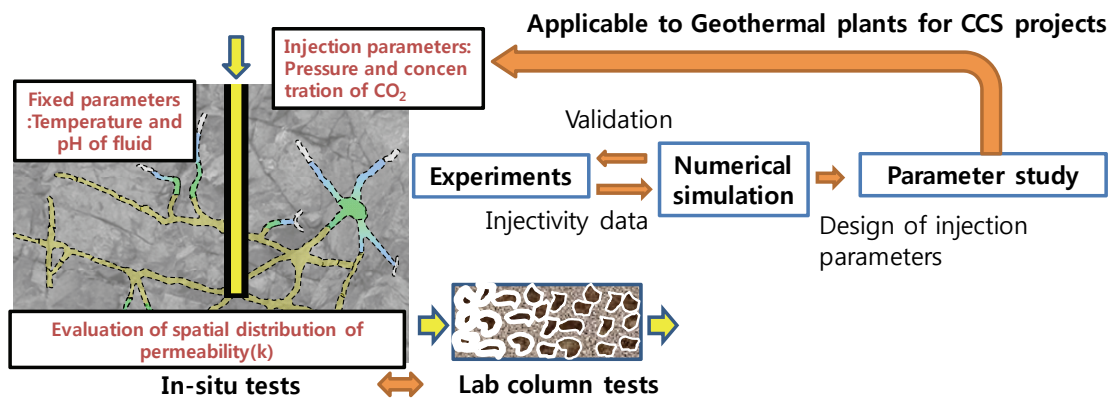
Fig. 1.2: Schematic diagram for research objectives in this dissertation.

In Chapter 3, the in-situ and laboratory scaled column tests at different pH and temperatures were performed to observe flow rates or permeability changes due to the carbonate precipitation. Test results show that clogging phenomena can be detected by the injectivity and pressure with the different temperatures and pH.

In Chapter 4, a step-wised numerical calculation method was introduced. The filtration ability and fluid flow velocity give us prediction of the amount of carbonate deposits with the distance from the inlet.

In Chapter 5, the sensitivity analysis for permeability and the amount of fixed carbonates has been suggested to determine the design parameters for CO_2 injection how far and how much the mineral particles will retain in the porous media.

Finally, the conclusion of this research is described in Chapter 6.
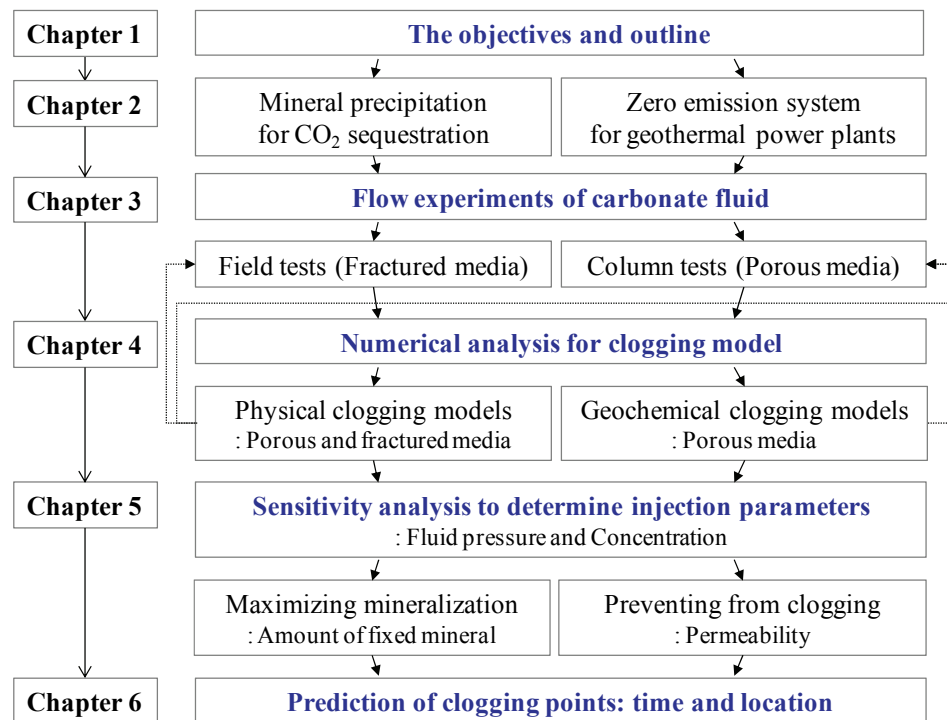
Fig. 1.3: Flow chart of the research in this dissertation.

CHAPTER 2   LITERATURE REVIEW

2.1   Numerical simulation for mineral precipitation

Numerical simulation is possible to reproduce for precipitation observed in laboratory-scale experiments and predict long-term behaviors. Most simulations can be classified into two main categories, chemical equilibrium model for a batch system and advection-reaction model for a flow system. The scale problem is a sensitive issue for precipitation process due to decreased porosity and permeability. McDowell-Boyer et al. (1986) highlighted the particle migration through porous media in subsurface environments. Thus, advection-reaction model can take advantage of prediction for the long-term time scale and apply to the various subject areas including grouting technology, petroleum engineering and geothermal fields.

The precipitation process is generally governed by the filtration phenomena as the first-order rate law (Ives, 1975). For the cement-based grouting, the particle filtration phenomenon is known to limit the infiltration of cement particles owing to clogging within the soil matrix. In reality, the filtration coefficient, which governs the filtration phenomenon, varies with the concentration of grout suspension and with the characteristics of the porous media including the porosity and pore size distribution of soil matrix (Reddi and Bonala, 1997). Kim et al. (2009) performed a series of pilot-scale chamber injection tests in order to verify the developed step-wise numerical calculation and to evaluate how cement-based grout can penetrate in the porous media.

The clogging problems is also of concern to the petroleum engineering from the standpoint of a rapid decrease in permeability and recovery of hydrocarbons. Hydraulic fracturing is a stimulating method to extract petroleum efficiently from low permeability

reservoirs. Sized particles (i.e. proppants) mixed with fracturing fluids are injected while maintaining fractures open. Stress-enhanced dissolution of proppant increases the density of grain packing and re-precipitation of mineral clogs pores (Lee et al., 2010). Gruesbeck and Collins (1982) suggested a simple model to describe not only filtration but also entrainment phenomena.

Mineral deposits in geothermal fluid are commonly found in subsurface fracture system. Lee et al. (1996, 1999) have refined the model for calcium carbonate mass transport in subsurface carbonate rocks of Morse and Mackenzie (1993) and developed a new experimental system capable of simulating calcite precipitation in veins to determine the influences of flow velocity and initial solution saturation state. Kato et al. (2000) studied fluid composition in the wellbore and fluid flow data using advection-reaction model to understand the mechanism of anhydrite scale at Sumikawa, Japan. Itoi et al. (1987) developed the numerical model to simulate permeability decrease caused by silica deposits in the reservoir near an injection wellbore. They carried out sensitivity analysis with the deposition rate coefficient (β_1) which was determined by trial and error method and fitting calculated flow rate to measured one. However it has little understanding about the physical and chemical meaning. For the $CaCO_3$ crystal growth, the size of particle obtained from supersaturated solutions was in a few of micrometers (Jada and Pefferkorn, 2000). This results mean that $CaCO_3$ particles have high surface areas per unit mass, which results in significant filtration potential and permeability change by clogged pore throats. Xu et al. (2004a) takes account of reactive surface areas of mineral in the reactive transport modeling to simulate precipitation of amorphous silica and injectivity loss in the Tiwi geothermal field, Philippines.

2.2   Zero emission system for geothermal power plants

Geothermal power plants extract steam produced from geothermal reservoirs in order to generate electricity. There are two power plant types, flash steam and binary cycle, which depend on the state of the hydrothermal fluids (steam or water) and its temperature. Flash steam plants are the most common type of geothermal generation plants in operation today. Fluid at high temperatures more than 182°C is pumped under high pressure into a flash tank at lower pressure, causing some of the fluid to rapidly vaporize, or flash. The vapor then drives a generator with a turbine. CO_2 emissions from geothermal power plants to the atmosphere are different from the CO_2 concentration of hydrothermal fluid. Muraoaka (2010) estimated CO_2 emissions of 18 geothermal power plants in Japan based on CO_2 concentration of steam in production wells as shown in Fig. 2.1. Estimated results presented that maximum CO_2 emissions of geothermal power plants are 20% less than those of LNG power plants.
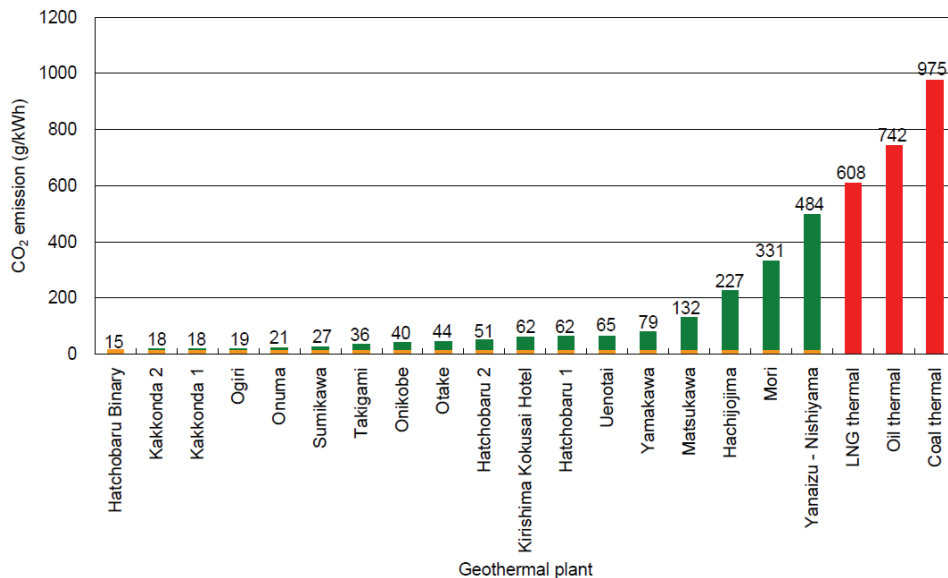
Fig. 2.1: CO_2 emissions in geothermal power plants in Japan (after Muraoka, 2010).

In order to make geothermal power plants more competitive in the renewable energy, it is essential to aim for zero emission of gas such as CO_2 and H_2S with binary cycle power plants as shown in Fig. 2.2. Binary geothermal power plants differ from flash steam systems in which water or steam from the geothermal reservoir never comes in contact with the turbine/generator units. Lowly to moderately heated (below 200°C) geothermal fluid and secondary fluid (typically a butane or pentane hydrocarbon) with a much lower boiling point than water pass through a heat exchanger. Heat from the geothermal fluid causes the secondary fluid to flash to vapor, which drives the turbines and subsequently, the generators. Binary cycle power plants are closed-loop systems and virtually nothing except water vapor is emitted to the atmosphere.
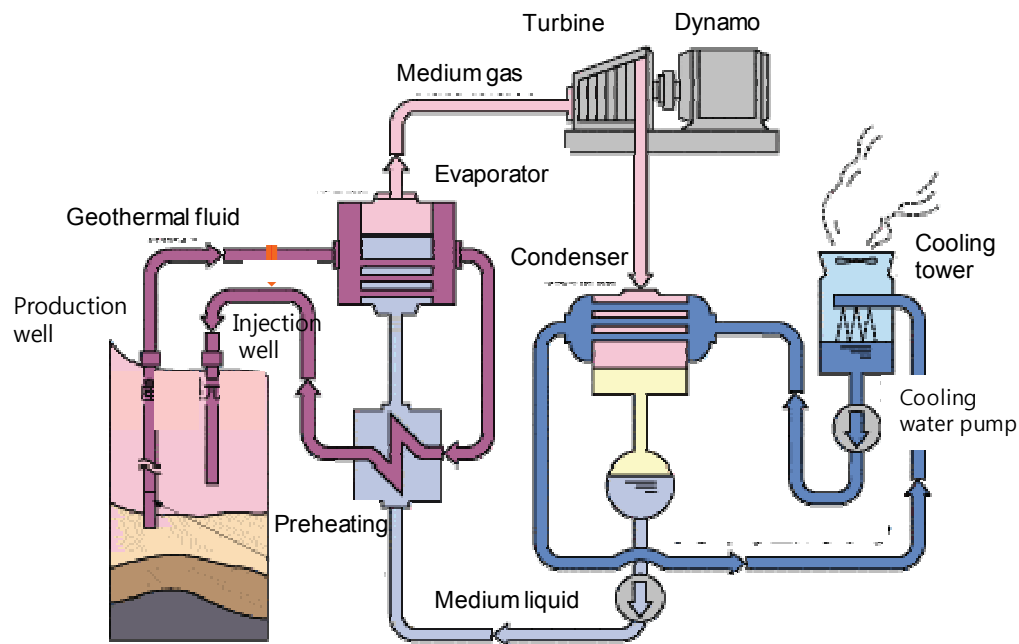
Fig. 2.2: Zero emission type of binary cycle system.

2.3   Summary

The chemical reaction rate of CO_2 with the rock becomes faster and precipitates the carbonate mineral easily as rising the reaction temperature. The deposited scale has provided serious problems especially in the binary cycle system for geothermal power plants because once again injected hydrothermal fluids will become supersaturated with respect to carbonates in the production well. Gas-liquid separation by flashing may increase pH of fluid with degassed CO_2 and finally carbonate scales will precipitate.

The research opportunity in this dissertation has begun to solve the scale problems in the hydrothermal conditions. Thus, geochemical clogging model will provide insights to estimate the amount of scale deposition and predict the clogging point with respect to elapsed time since injection and location of reservoirs.

CHAPTER 3   FLOW EXPERIMENTS OF CARBONATE FLUID

3.1   Field experiments at the Hot Dry Rock (HDR) site

3.1.1   Introduction

The basic idea of this research aims to accelerate growth of the artificial carbonate which can prevent CO_2 from leaking and facilitate CO_2 storage in areas with no continuous cap rock. Ca^{2+} released from rocks might be removed as calcium carbonate ($CaCO_3$) during CO_2 injection into relatively high-temperature fields as shown in Fig. 3.1 (Ueda et al., 2005). The chemical reaction rate of CO_2 with the rock becomes faster and precipitates the carbonate mineral easily as rising the reaction temperature. On the contrary to benefit of self-sealing, injectivity might decrease with time due to clogging reservoirs. Therefore, field experiments were performed to study what is the key point for clogging mechanism to locate carbonate deposits as far away from the inlet as possible.
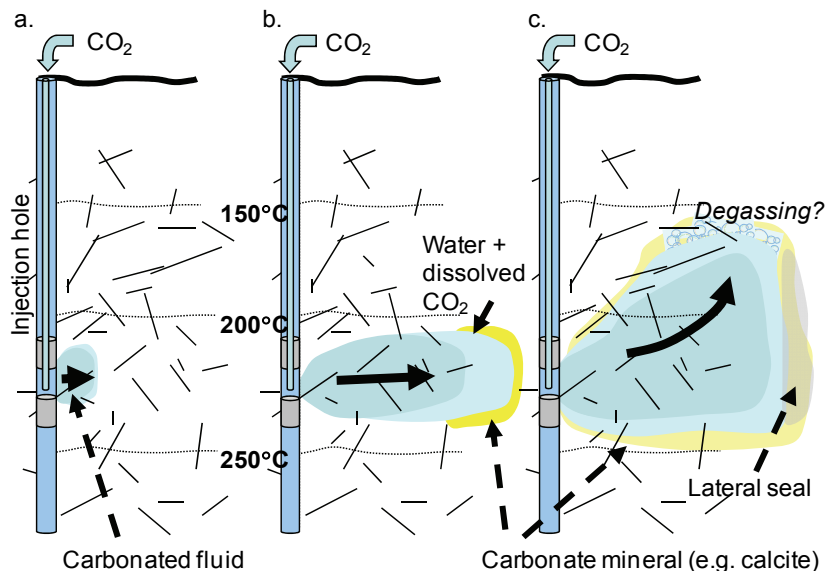
Fig. 3.1: Concept of carbonate mineralization at hydrothermal conditions. (a) The vicinity of injection hole (b) Water-CO$_2$ mixture zone (c) Peripheral sealing zone

13

The supersaturated fluid with respect to $CaCO_3$ were injected into a high temperature zone through a wellbore, OGC-2, at the Ogachi Hot Dry Rock (HDR) geothermal site in Japan (Kaieda et al., 2005). At the Ogachi site, three wells (OGC-1, 2, 3) were drilled into granitic rock to a depth of 1,100 m (Fig. 3.2). OGC-2 was cased with full-hole cementing from the ground surface to a depth of 700 m and below 700 m to the bottom-hole was left uncased (open hole). A total of 899 open-type fractures was found by bore hole televiewer (BHTV) (Ito et.al, 1999). The bottom-hole diameter is 98mm. Water level in OGC-2 is 150 m below the ground surface.

These were used initially for field experiments into HDR geothermal energy extraction, and later for studies of geologic storage of CO_2. The bottom-hole temperature at a depth of 1,100 m was measured around 240 ˚C. The bedrock below 300 m from the surface consists of pre-Tertiary granitic rocks and mylonite, which underlines Neogene and Quaternary felsic volcanic rocks.
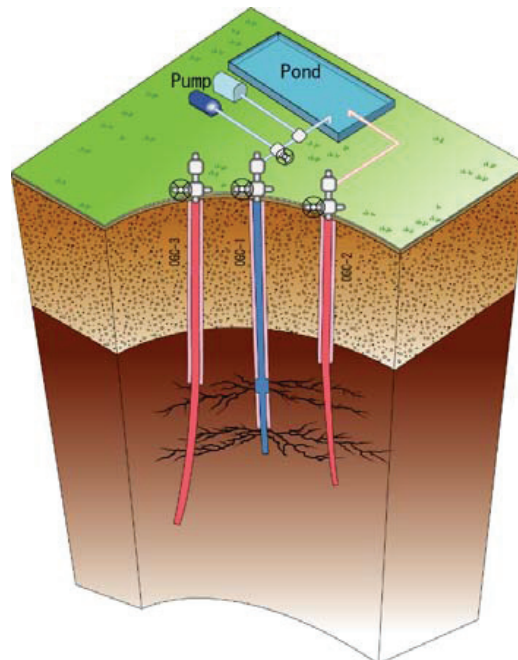
Fig. 3.2: Schematic diagram of wellbore configuration at the Ogachi Hot Dry Rock (HDR) geothermal site (after Kaieda et al.,2005).

3.1.2   Experimental procedure

Ogachi field experiments reported that Ca from rocks might be removed as calcium carbonate during CO_2 injection into hydrothermal reservoirs. However, there are not enough Ca released from rocks to clog pores with carbonate precipitation within a short period of time. For this reason, neutralized river water mixed with 500 mg/L $CaCl_2$ and 620mg/L CO_2 (dry ice blocks) had been injected for about one week. The mixed fluid shows undersaturated with respect to calcite under pH 5. In order to adjust pH, NaOH was added into tank to promote carbonate precipitation under hydrothermal reservoirs without scaling troubles on water level gauge. The saturation index (S.I.) is defined in the following equation:

$$S.I. = \log\left(\frac{Q}{K_{sp}}\right) \tag{3.1}$$

where Q is the ion activity product and K_{sp} is the solubility product of mineral for the chemical reaction. Positive, zero, or negative S.I. values indicate mineral supersaturation, equilibrium, or undersaturation, respectively. Saturation indices with respect to calcite were calculated by the USGS computer code, PHREEQC (Parkhurst and Appelo, 1999) to maintain supersaturated (S.I. > 0) at a depth of 950m (200 ˚C) and undersaturated (S.I. < 0) at a depth of 150m (55˚C) (Table 3.1). According to calculation of S.I., the pH of injection fluid is desirable to be at the range of from 5.5 to 5.9 including the effect of decreasing temperature by injection. Na concentration of the solution as NaOH was calculated by taking the ion balance.

8.89kg $CaCl_2$ and 8.89m^3 water were mixed into two tanks to keep $CaCl_2$ 1000mg/L (Fig. 3.3). In order to dissolve CO_2, 40kg dry ice blocks are added into the mixed fluid in the tank 1. After CO_2 was totally dissolved, pH was 4.6. Finally, NaOH

was added into this fluid which was shown as pH 5.9. The same procedure was repeated for the tank 2 as well. This system is possible to inject supersaturated fluid with $CaCO_3$ from tank 1 to OGC-2 continuously at constant flow rate. The amount of injection fluid in one cycle including 23 hours injection and 1hour shut-in was considered enough to remain water level up to 20 cm height of tank.

Field experiment was carried out in the following steps (Table 3.2). Temperature logging and sampling water using geochemical sampler were performed to understand the initial state of fluid prior to injection. Injection flow rate was constant at 10L/min. On 16th October, the second temperature logging and sampling with a geochemical sampler were tested while injecting water dissolved CO_2. In addition, the fluid was replaced with fresh water in the casing in order to prevent the casing of OGC-2 wellbore from corrosion after the end of sampling tests. At the end of the injection carbonate fluid, the third temperature logging and sampling tests were carried out again during from 8th to 9th November. Injection of fresh water was finally done for the permeability test.
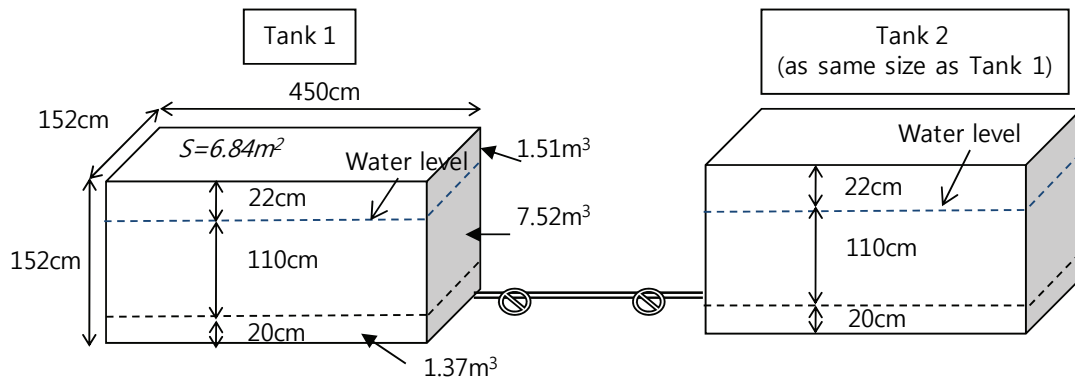
Amount of fluid in a tank= (20+110)x6.8=8.89m³

Fig. 3.3: Schematic diagram of two tanks for fluid injection.

Table 3.1: Calculation of pH and saturation index with temperatures.

pH					S.I. of calcite					NaOH
15°C	55°C	100°C	150°C	200°C	15°C	55°C	100°C	150°C	200°C	mg/L
4.30	4.20	4.31	4.55	4.50	-3.41	-3.00	-2.40	-1.65	-1.53	-
5.00	4.85	4.98	5.24	5.22	-2.09	-1.72	-1.09	-0.30	-0.16	65.5
5.50	5.35	5.48	5.75	5.84	-1.15	-0.78	-0.15	0.63	0.87	221.1
5.90	5.75	5.88	6.16	6.40	-0.46	-0.10	0.52	1.30	1.64	485.9
6.00	5.85	5.98	6.26	6.54	-0.30	0.06	0.68	1.45	1.80	575.1
7.00	6.84	6.92	7.17	7.52	1.01	1.34	1.87	2.53	2.84	1505.9

1) $CaCl_2$=1000 mg/L, CO_2=2000 mg/L.
2) Temperature at a depth of 150 m and 950 m is 55 ˚C and 200 ˚C, respectively.

Table 3.2: Procedure for the Ogachi field experiments.

3.1.3   Results and discussion

CRIEPI (Ito et al., 2011) measured the change in flow rate and ground water level in OGC-2 wellbore during injection of carbonate fluid (Fig. 3.4). The ground water level corresponded well with the change of injection flow rate. When the injection was started, the water level was rising about 10 m immediately and vice versa. Fig. 3.5 shows the results of temperature logging data in OGC-2 wellbore. The temperature before carbonate fluid injection and after twenty-three days from the end of the experiment is approximately equal each other. Temperature during fluid injection decreased from 210 ˚C to 188 ˚C at a depth of 950 m in which a geochemical sampler was installed. In order to evaluate the permeability around OGC-2 wellbore, we used the following equation (Hvorslev, 1951):

$$k = \frac{Q}{2\pi L \Delta h} \ln\left(\frac{L}{r}\right) \qquad (3.2)$$

where k is the permeability (m/s), Q is the flow rate (m^3/s), L is the length of test section (m), Δh is the differential head, r is the diameter of the open-hole (m).
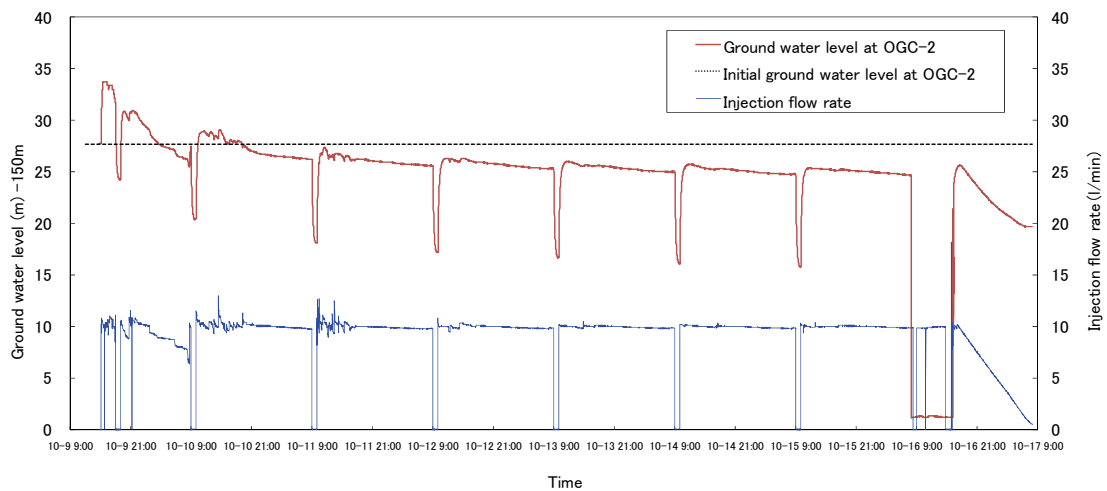
Fig. 3.4: Monitoring of flow rate and groundwater level (after Ito et al., 2011).

18

Drawdown per a cycle including injection and shut-in tended to be getting larger with respect to the elapsed time since injection. Permeability around OGC-2 borehole can be estimated from the stable fluid pressure about two hours later from the injection. Water level was lowering from -115m to -125m from 9th to 16th October because there is one possibility the density of pore fluid were increased by cooling effect with carbonate fluid injection. According to the temperature logging results before and after the carbonate fluid injection, the temperature was reduced by 20 ℃ over the eight days injection. Thermal expansion coefficient of water (β) indicates linear relationship in the range from 20 ℃ to 200 ℃ so that the average one as 0.0008 can be adopted in the following equation:

$$V = V_0(1+\beta\Delta T) \tag{3.3}$$

where V, V_0 is the volume after change of temperature and initial volume (m^3) and ΔT is differential temperature. Height of water column can be expressed by dividing volume by the cross-sectional area of borehole in the following equation:

$$H = H_0(1+\beta\Delta T) \tag{3.4}$$

where H_0 is the initial height of the water column and H is the height of water column after change of temperature, ΔT.

When the datum of ground water level is -950m, initial ground water level before injection (-123 m) becomes 827 m as H_0. H with ΔT = -20 ℃ can be calculated as 814 m, thus, ground water level eight days after injection can be estimated as -136 m (= -950+814). Drawdown of 13 m by this estimation is larger than maximum drawdown (9.61 m) observed during in-situ experiments.

The changes of groundwater level and injection flow rate discussed about two key results with the permeability change in Fig. 3.6.

1.   Permeability decreased drastically on the first day from the injection. This is consistent with the result that the growth of calcite by the recovery of temperature after the water injection (Kaieda et al., 2009).

2.   Permeability was recovering from relatively low permeability to the initial permeability after about 1 month from the pause of injection as groundwater turned to the unsaturated state with respect to calcite.
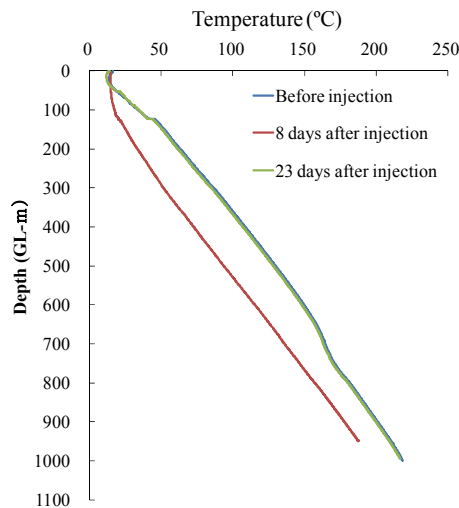
Fig. 3.5: Temperature logging data at OGC-2.
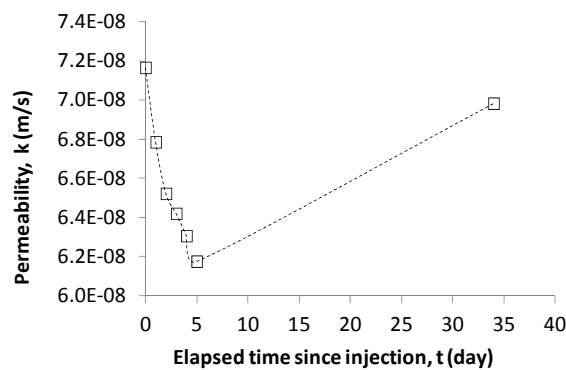
Fig. 3.6: Permeability change during field experiments.

3.2   Laboratory scaled column experiments

3.2.1   Introduction

A single reservoir measurement at Sleipner indicates a temperature at the injection point of about 36°C. Under such conditions, CO_2 will keep in stable as a supercritical phase due to slow reaction rates in reservoir rocks (Bickle et al., 2007). In the other site at Nagaoka, though the injected CO_2 was in a supercritical state under the temperature of formation water (48.8 °C), the observed chemical composition and the reservoir modeling implied that mineral trapping regarded as one of the alternative geologic sequestration could occur from the early stage of CO_2 storage (Mito et al., 2008). This means that reaction rates of carbonate mineral is faster than those estimated by IPCC (2005).

Carbonate mineral is commonly found as hydromagnesite at low temperature in ultramafic region as shown in Fig. 3.7 (RITE, 2008) and calcite at high temperature in the Ogachi Hot Dry Rock (HDR) geothermal site as mentioned before. However there is little information how permeability change in reservoirs by chemical reaction of CO_2 with reservoir rocks. For this reason, carbonate fluid flow experiments help us to understand mechanisms of carbonate precipitation under not only relatively high temperatures but also room temperatures.

Fig. 3.7: A serpentinite core sample with carbonate at Hidaka, Hokkaido (after RITE, 2008).

3.2.2   Experimental setup

Laboratory scaled tests were performed under three different temperature cases because growth rates of mineral are generally proportional to saturation index (S.I.) that depends on temperature and pH.

As shown in Table 3.3, the saturation indices (S.I.) of minerals in experimental solutions were calculated by PHREEQC in order to obtain a further insight into the chemical reactions at the various range of temperatures (20~185 ºC). The thermodynamic database llnl.dat, which is distributed with PHREEQC, was used. A positive and negative S.I. indicates a potential for precipitation and dissolution, respectively.

Table 3.3: Chemical compositions for fluid sampling at three cases.

Chemical compositions	Ogachi	Matsushiro	Namikata
Date of observation	2010.10.16	2010.12.15	2009.10.24
Temperature of fluid sampling (ºC)	15.1	22.1	20.2
Temperature of fluid inside column (ºC)	185	49	20
pH	6.2	6.7	11.3
EC (mS/m)	249	2700	46
Na (mg/L)	190	4300	47
K (mg/L)	0.5	450	2
Ca (mg/L)	280	850	18
Mg (mg/L)	0.6	280	0.2
Sr (mg/L)	-	14	-
Cl (mg/L)	320	8600	66
SO_4 (mg/L)	9	210	7.5
SiO_2 (mg/L)	28	170	12
Al (mg/L)	0.1	-	0.8
Fe (mg/L)	5.2	11	0.007
Mn (mg/L)	0.07	1.3	< 0.001
Total CO_2 (mg/L)	620	1800	13
S.I. of calcite / aragonite	1.71 / 1.56	0.99 / 0.85	0.96 / 0.82

The case at Ogachi

Almost the same experiment was performed under conditions similar to the Ogachi HDR geothermal site, Japan. The equipment setup is illustrated in Fig. 3.8. The column consists of a cylindrical chamber with the inside diameter of 4 cm and the height of 50 cm. A section of granodiorite core (from 998 m depth in the Ogachi production well) was crushed and sieved to 1-2 mm diameter rock cuttings. These rock fragments, whose density is 2.66 g/cm^3, were packed into the column. The porosity of column with rock cuttings was measured at 0.27, which was also derived the volume of saturated water and the closed-packing column. The injection pipe was positioned at the top of the column and fluid flowed downward at 5.5 cm^3/s as the initial flow rate for four days. Flow rates, temperature, and pressure within the column were monitored every hour. Differential total head between the inlet and the outlet was 5 kPa regarded as 50-cm-length column. In the column, average temperature was kept constant at 185 °C and fluid pressure showed a gradual increase from 2 MPa to 6 MPa.
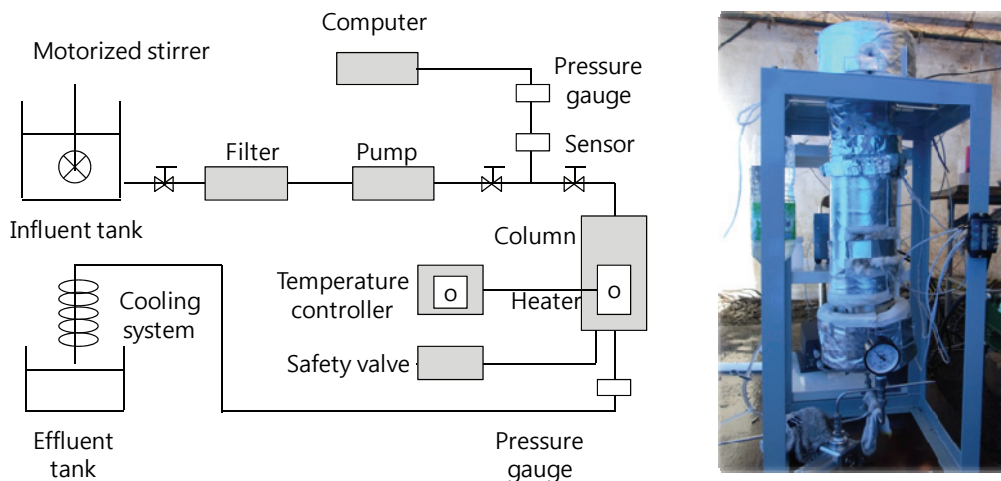
Fig. 3.8: Experimental setup for the column test at Ogachi.

The case at Matsushiro

Carbonate fluid from the Matsushiro hot spring in Nagano Prefecture, Japan, was suitable for our column tests as fluid was supersaturated with carbonate mineral at neutral pH (=6.7). This fluid was injected into the column at 49 °C during about two days (= 43 hours). Experimental conditions are shown in Table 3.4 under three cases. Differential total head (Δh) in cases of C1 and C2 was kept same value. But only the case for C1 was sterilized the hot spring fluid with ultraviolet light irradiation in order to inhibit acceleration of carbonate mineral precipitation by bacteria in hot spring fluid. The C3 case at Δh= 42 cm was compared with C2 case at Δh= 50 cm.

The equipment setup is designed to change the deferential total head (Δh) and flow rate (Q) by adjusting points of overflow and discharge fixed as shown in Fig. 3.9 (a). The SUS column consists of a cylindrical chamber with the inside diameter of 4.3 cm and the height of 40 cm. For the column experiments in 2010, seven manometers at intervals of 5 cm were installed on the side of columns to indicate the pressure head by the difference in fluid levels at each locations.

In order to measure the pressure automatically in 2011, fluid pressures at each point of 5 cm, 10 cm, 15 cm, 25 cm, 35 cm was measured with digital pressure sensors (Fig. 3.9 (b): Keyence, GP-M010). The column is packed with glass beads which are 2 mm average in diameter and 2.50 g/cm^3 density. The initial porosity of this packed column was 0.39 which was determined by the volume of water in pore and the volume of the column. It is convenient for numerical calculations to adopt glass beads because they are spherical shapes and density is almost the same as the rock.

Table 3.4: Experimental conditions for column experiments.

Experimental Case	Diameter of glass beads, ϕ (mm)	Differential total head, Δh (cm)	Initial flow rate, Q_0 (L/min)	Hydraulic gradient, i (-)	Initial permeability K_0 (cm/s)
C1	2	50	1.1	1.25	2.0
C2	2	50	1.3	1.25	2.4
C3	2	42	0.90	1.05	2.0
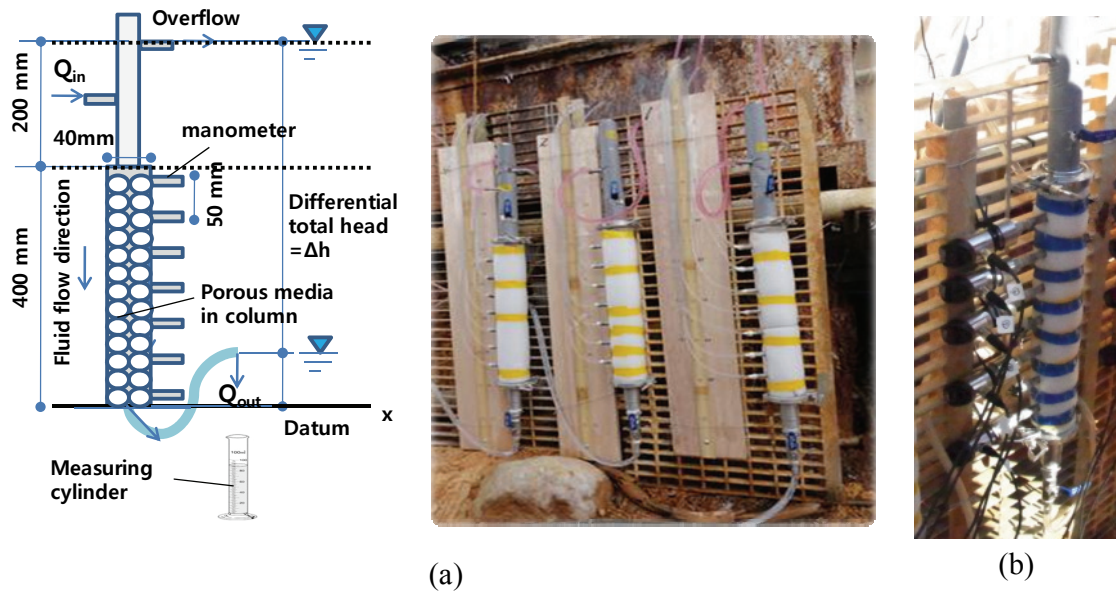
Fig. 3.9: Experimental setup for the column test at Matsushiro.
(a) Using the manometers (b) Using the digital pressure sensors

The case at Namikata

The groundwater enriched in $CaCO_3$ from a tunnel at Namikata LPG stockpiling base in Ehime Prefecture, Japan, (Oriyama et.al, 2007) was used for our column test and showed high pH (= 11) due to interaction with cement. In the tunnel, there is so much carbonate precipitation that we used one of the groundwater with high pH for our experiments. This fluid flowed into the column at 20 °C for twenty-five days and the initial flow rate was 13.3 cm^3/s.

The equipment setup is designed to maintain the deferential total head (Δh= 100 cm) constant by keeping points of overflow and discharge fixed as shown in Fig. 3.10. The column is a rectangular, parallel piped chamber with 50-cm-long sides and 4 cm square on a side. The column is packed with glass beads which are 2 mm average in diameter and 2.50 g/cm^3 density. The initial porosity of this packed column was 0.29 which was determined by the volume of water in pore and the volume of the column. Both top and bottom of the column are covered with filters to render the glass beads immovable.
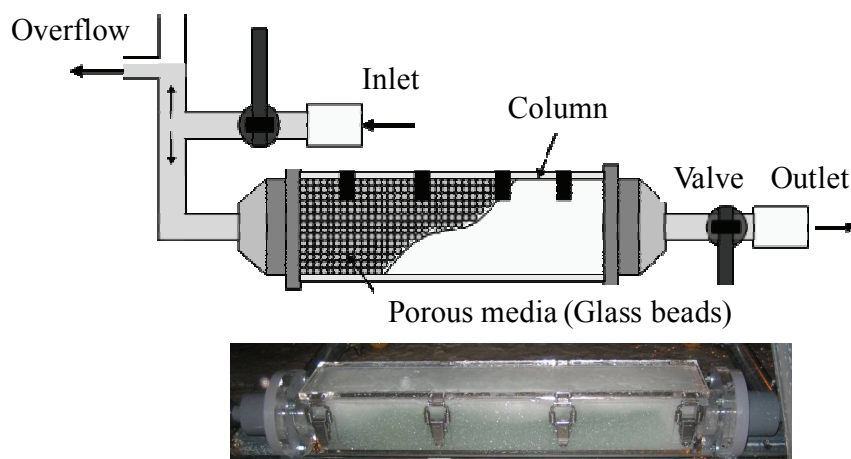
Fig. 3.10: Experimental setup for the column test at Namikata.

3.2.3   Analysis methods

XRD analysis

Mineralogical analysis of the precipitation formed in powder was carried out using X-ray diffraction (Bruker, MXP-18HF + MDG) with Cu radiation energy source and 1.54 Å wavelength. XRD scanning was performed in the range of from 6° to 70° (0.071 step width). As it was difficult for the sample in Ogachi to extract only the deposits of rock samples, samples were crushed in an agate mortar until about 6.7cm from the inlet of column. On the other hand, for the samples of Matsushiro and Namikata, deposits attached to the surface of the glass beads from the inlet to 10cm were collected rubbing lightly with a sieve.

ICP-AES and SEM analysis

In order to analyze the mass of the calcium that adheres to the surface of the porous media, each 4 g samples extracted from any ranges of column in a 100 ml beaker were dried at 70 °C in an oven for about one day. After weighing the samples, in order to dissolve chemical composites of precipitation, remaining samples were mixed with small amount of hydrochloric acid solution (HCl) 12 mol/l in the beaker for several hours. This filtered fluid added to distilled water until 50ml were collected as a certain amount and diluted twice with a solution of nitric acid (HNO_3) 4 % to measure Ca concentration with ICP-AES (HP-4500 series). For the observation of the sample surface and shape of the deposit, samples were picked randomly in the column using SEM (KEYENCE, VE-7800).

3.2.4   Results and discussion

Amount of total Ca defined as the mass of Ca particles deposited per initial unit pore volume was measured by ICP-AES as shown in Fig. 3.11. For the case at Ogachi and Namikata, the amount of Ca decreased exponentially with distance from the inlet due to low initial fluid velocity (u= 1.6~1.8cm/s). On the other hand, the amount of Ca in deposits was distributed with respect to distance uniformly for the case at Matsushiro because of relatively higher initial fluid velocity (u= 4.8 cm/s). From these results, the fluid flow velocity can govern the distribution of the amount deposits.
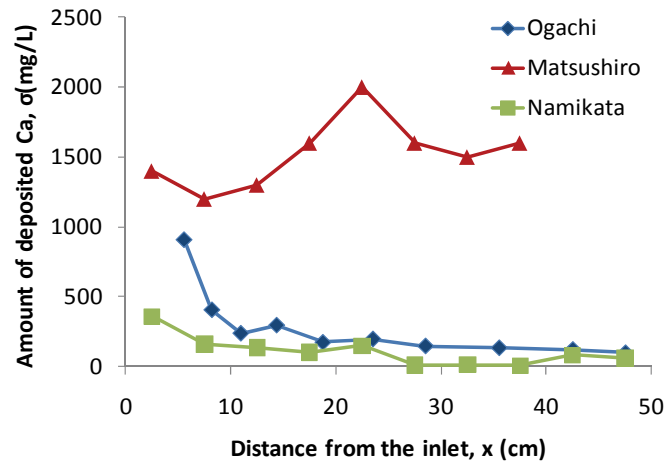
Fig. 3.11: Amount of deposited Ca with distance from inlet
(Matsushiro case corresponding to C3 case).
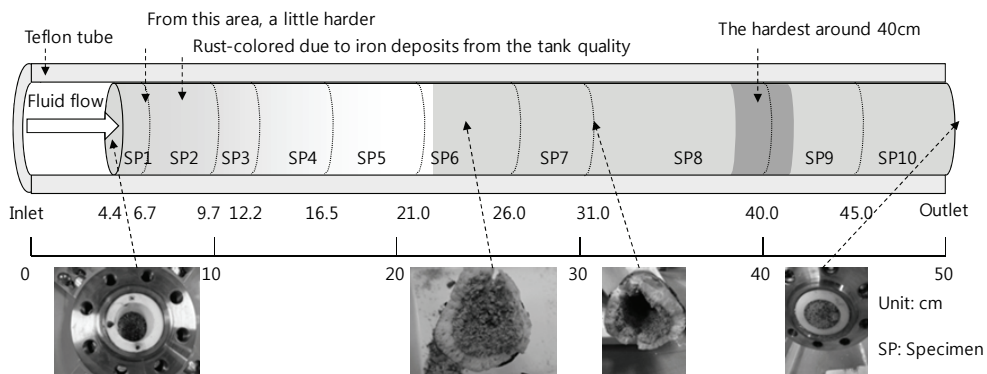
Fig. 3.12: Calcite and portlandite precipitation after the column experiment.

The case at Ogachi

Rock cuttings include no calcite ($CaCO_3$) before injection. After injection, deposits identified as both calcite and portlandite or calcium hydroxide ($Ca(OH)_2$) were found in the column (Fig. 3.12) at Ogachi by XRD analysis of samples until 6.7 cm from the inlet of column (Fig. 3.13). As shown in Fig. 3.14, identified calcite particles were found on the irregular surface of rock cuttings using SEM. Portlandite precipitated in the center part of the column might affect the observed permeability change, whereas calcite was distributed through the porous media uniformly. These results implied that estimated growth rates of carbonates might include portlandite and calcite. High temperature high pressure column experiments have difficulty in keeping constant temperature evenly, temperature on the inside of column might exceed 250 °C temporarily and locally. The kinetic model described the behavior of the dehydration reaction of calcium hydroxide in the range of temperatures 330-450ºC (Irabien et al., 1990). The effect that solubility of calcite decreases with increasing temperatures (Chiba, 1991) means that precipitation will occur immediately at high temperatures. The variations in temperature inside the column would impact precipitation rates to have advantage of clogging phenomena with elevated temperature. This effect corresponds to the results that deposits clog porous media with deposited Ca (Fig. 3.11).

As shown in Fig. 3.15, fluid flow test was performed continuously while maintaining the average temperature at 185 °C using heater and temperature controller. Flow rate declined up to 12% of the initial flow rate for about four days. Pressure in the high-temperature high-pressure apparatus increased from 2 MPa to 6 MPa gradually. The observation of pressure and flow rate suggests that the detection of clogging mechanism may have been effective.
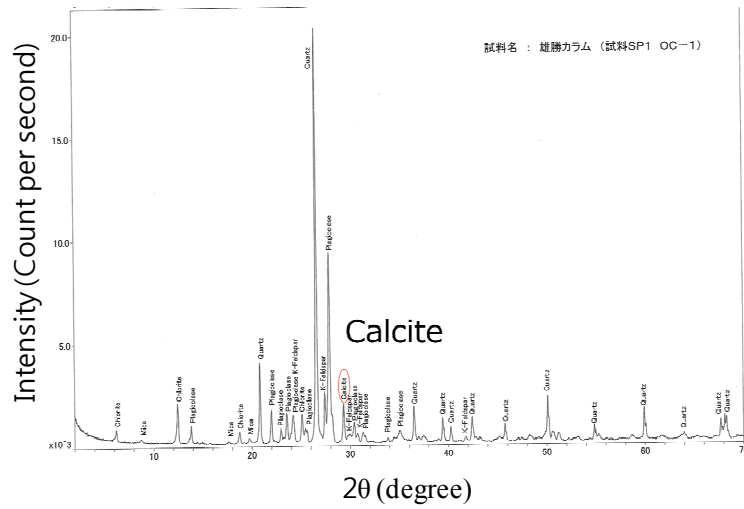
Fig. 3.13: XRD analysis result at Ogachi.
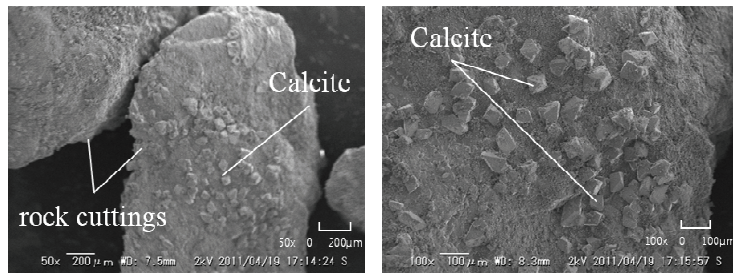
Fig. 3.14: SEM image analysis result at Ogachi.
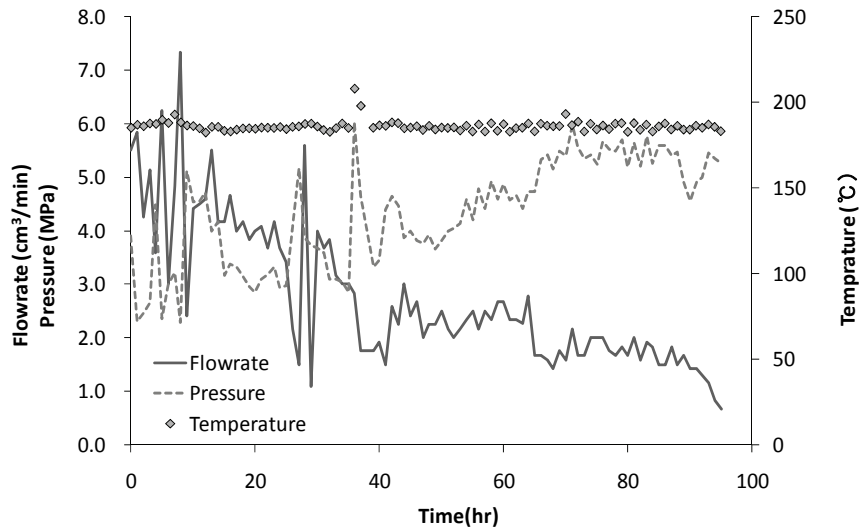
Fig. 3.15: Change of discharge flow rate, pressure and temperature at Ogachi.

The case at Matsushiro

Aragonite has been identified until 10cm from the inlet by XRD analysis (Fig. 3.16) without calcite. Aragonite as a polymorph of $CaCO_3$ tends to generate at a relatively high temperature and saturation. It is also possible that high concentration of magnesium (Mg) and sulfate (SO_4) with smaller ionic radius than Ca is attributed to the crystal growth of aragonite (Table 3.3). The previous research by Kitano et al. (1969) indicates that Mg ions favor the formation of aragonite, and hinder the formation of calcite and vaterite. As shown in Fig. 3.17 and Fig. 3.18, the spherical surface of reddish brown-colored glass beads was covered with aragonite as the layer growth. Surface condition of the porous media will be a dominant factor which affects the mineral growth rate. After column tests in all cases, glass beads were picked up at each 5 cm from the inlet. By dissolution with hydrochloric acid solution (HCl), the amount of deposited Ca and Fe was concentrated outstandingly around the inlet and distributed exponentially with respect to the distance from the inlet.
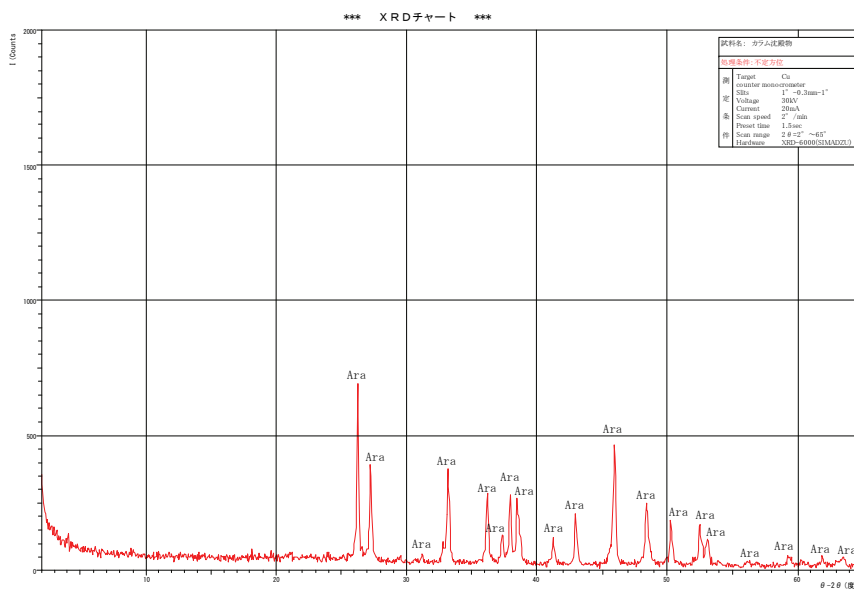
Fig. 3.16: XRD analysis results at Matsushiro (C3 case).
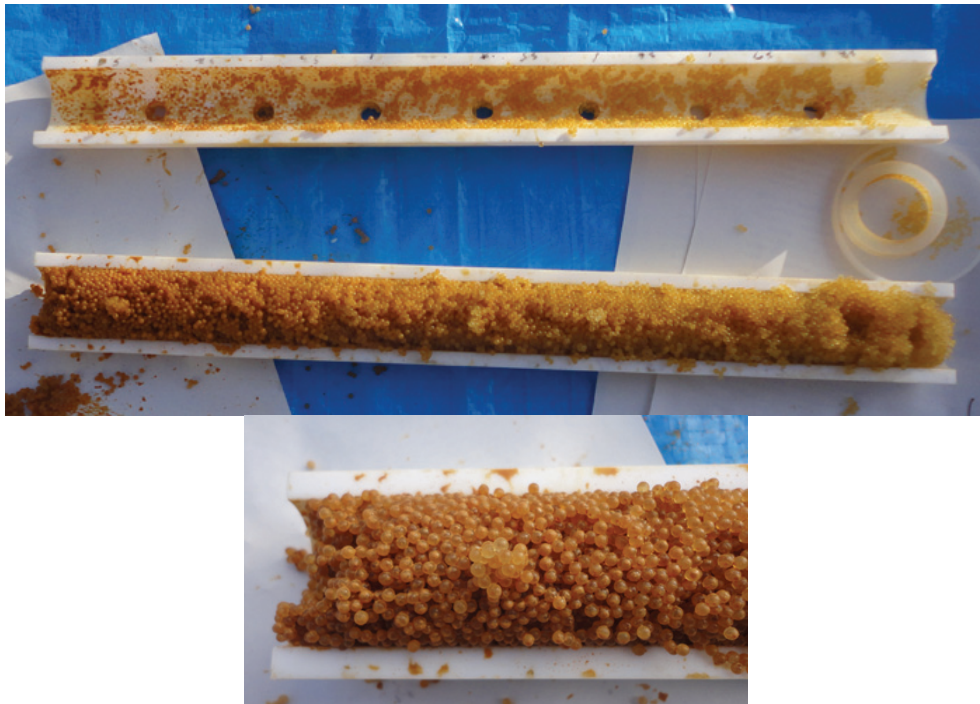
Fig. 3.17: Reddish brown-colored glass beads after column experiments at Matsushiro.
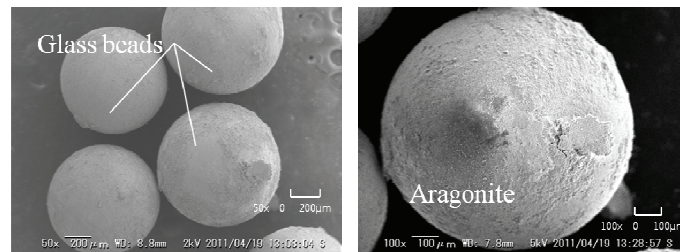
Fig. 3.18: SEM image analysis results at Matsushiro.

As shown in Fig. 3.19, flow rate in all three cases increased up for 6 hours because the gas-lock by CO_2 gas dissolved in hot spring fluid was mitigated with respect to injection time (Stage 1). Flow rate for two cases, C2 and C3, maintained constant flow rate during a day (Stage 2) and then began to decrease up to less 10% of the initial flow rate. However, flow rate results for the case 1 with sterilization showed linear decline earlier than other cases since Stage 2. It is known that this hot spring fluid contains metal ion which can slow down the growth rate of calcite crystals (Meyer, 1984) to varying

degrees. Ozone can be produced in hot spring fluid by sterilization with ultraviolet light. $Fe(OH)_3$ will be precipitated by reaction with ozone and Fe ion. There is a possibility to weaken the effect of inhibiting the carbonate precipitation with decrease of the Fe ion concentration in the solution in the column. The reason of decreasing flow rate is related to the deposition of $CaCO_3$ and Fe compounds on the surface of porous media occurs lower porosity and permeability.

Total head (h = pressure head (h_p) + elevation head from the datum (h_e)) distribution for all cases was measured by digital pressure sensors (Fig. 3.20). At the beginning point of injection, distribution of total head shows linear curve line because of no head loss in the column. When carbonate mineral precipitated in pores prevented the fluid from flowing smoothly since the injection time elapsed, distribution of total head changed into a non-linear curve from a linear one due to the head loss.
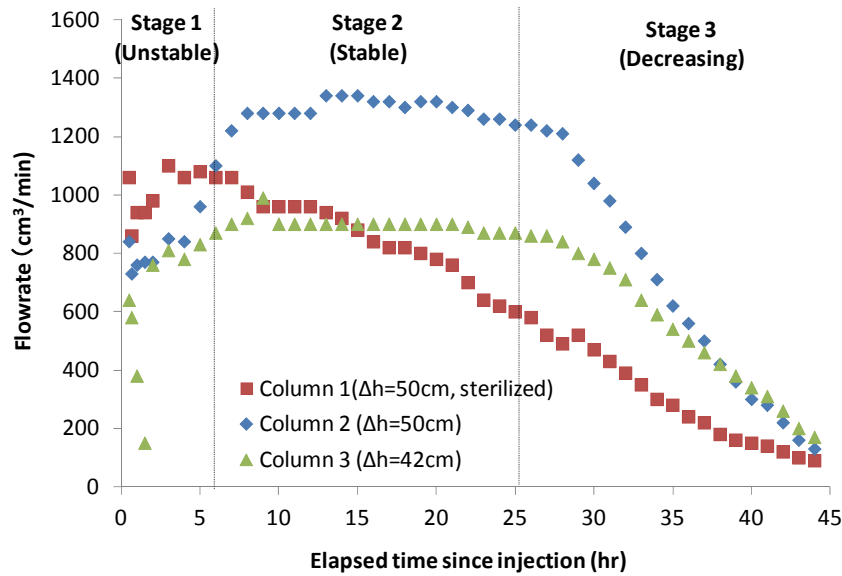
Fig. 3.19: Flow rate with elapsed time at Matsushiro.
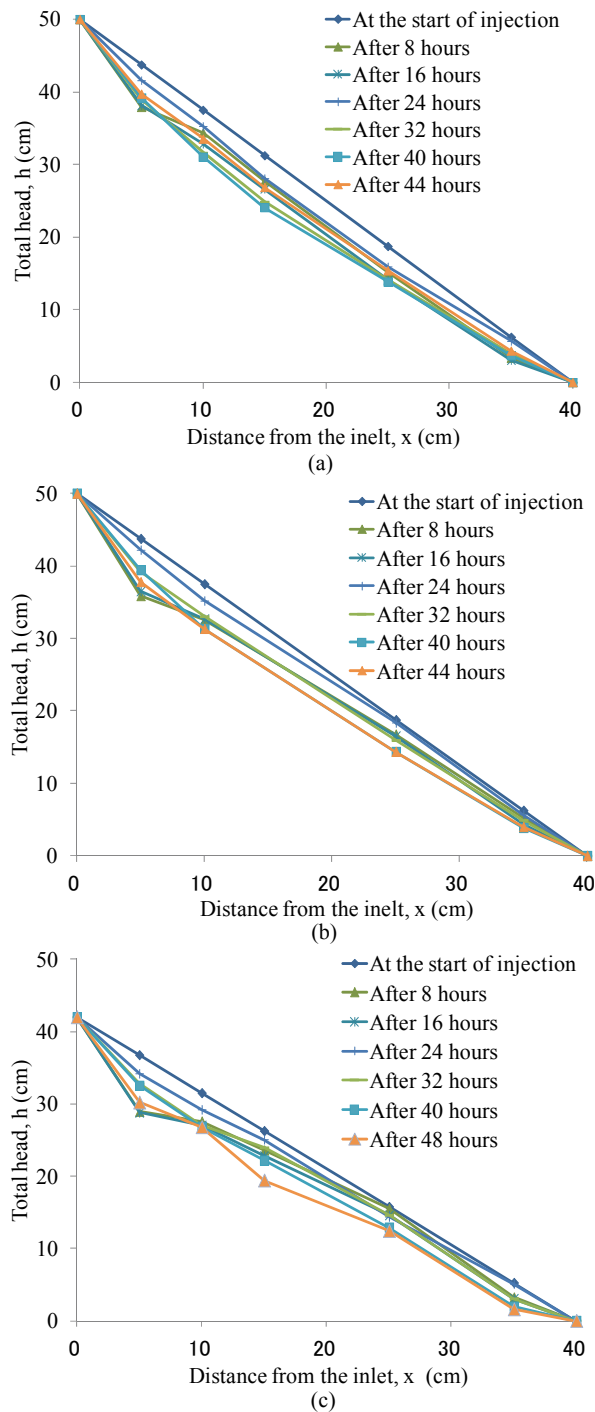
Fig. 3.20: Total head with distance from the inlet at Matsushiro.
(a) C1 (b) C2 (c) C3

The case at Namikata

34

From the results of XRD (Fig. 3.21), the calcite has been identified on the porous media at the Namikata LPG site. Accumulation of Ca shown to the middle of the column matched to the results that a lot of dendritic calcite crystals were observed by SEM analysis (Fig. 3.22). At the range of from the inlet to 5 cm, needle-shaped crystals have a large amount of fine calcite crystals. At the range of from 10cm to 15cm, crystal grain size has been enlarged. However, the more columnar calcite crystals than needle-shaped crystals were found from the middle section to the outlet.

Flow rate decreased by 5% of the initial flow rate within twenty-five days since injection (Fig. 3.23). Although differential total head was kept as 100cm, distribution of pressure in the column was not clear because of no installation of manometer on the column.
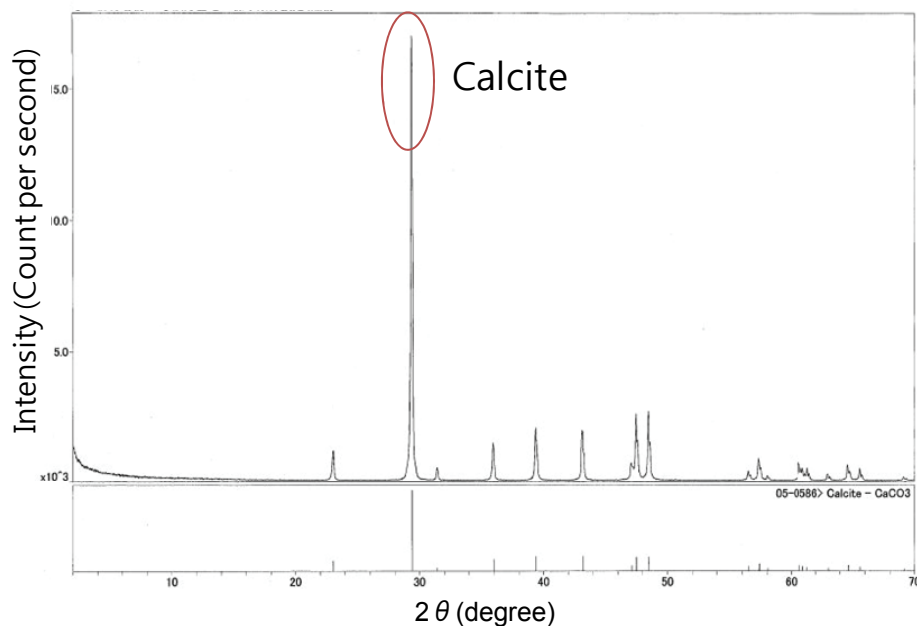
Fig. 3.21: XRD analysis results at Namikata.

(a) 0~5cm

(b)10~15cm

(c)15~20cm

(d)20~25cm

(e)35~40cm

(f)45~50cm
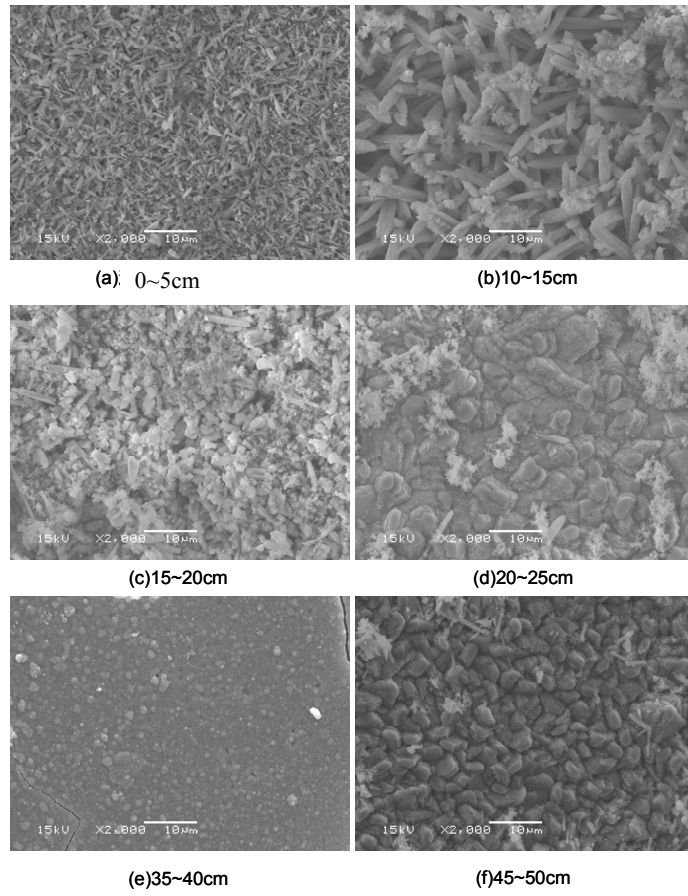
Fig. 3.22: SEM image analysis results at Namikata.
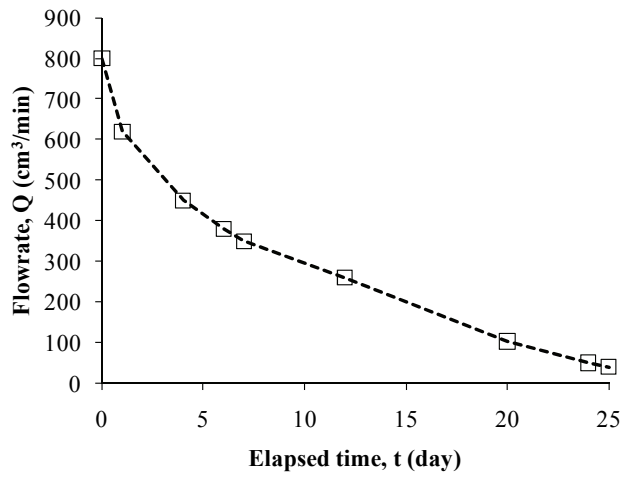
Fig. 3.23: Change of discharge flow rate at Namikata.

3.3   Conclusions

Flow experiments through porous media were performed using supersaturated carbonate fluid (Table 3.5) under three different cases of high (185 ºC), middle (49 ºC) and low (20 ºC) temperature. Fine-grained sedimentary rocks (e.g. sandstones) are porous enough to storage large quantities of CO_2 into reservoirs and the porosity of Berea and Tako sandstone showed 0.19 and 0.24 respectively (Kim et al., 2011). Therefore porous media such as rock cuttings and porous media was targeted at the large porosity (0.27~0.39) enough to precipitate carbonates in flow experiments. After injection of carbonate fluid, crystal growth of calcite and aragonite were found on the surface of porous media in all cases observed by SEM.

According to chemical kinetics, growth rates of mineral are generally proportional to saturation index (S.I.) that depends on temperature and pH. S.I. of carbonate mineral indicates higher values as pH becomes higher in despite of lower concentration of Ca^{2+} and HCO_3^- for examples in Namikata case. In addition, the concentration of reactants such as Ca and CO_2 can contribute directly to the crystal growth rate of carbonate mineral. The product of S.I. and CO_2 concentration for the in-situ test at Ogachi site can be expressed as a function of growth rates shown as Fig. 3.24 (Kuroda, 2009).

Table 3.5: Properties for carbonate fluid under different temperature cases.

Site	Temperature (ºC)	pH (-)	Ca (mg/L)	Total CO_2 (mg/L)	S.I. (-)	S.I. x [CO_2] (g/L)	Required time for clogging[*1] (day)
Ogachi	185	6.2	280	620	1.8	1.12	4
Matsushiro	49	6.7	850	1800	1.1	1.98	2
Namikata	20	11.3	18	13	1.1	0.0143	14

1) Required time for clogging was defined as duration when the flow rate declined up to 20% of the initial flow rate.
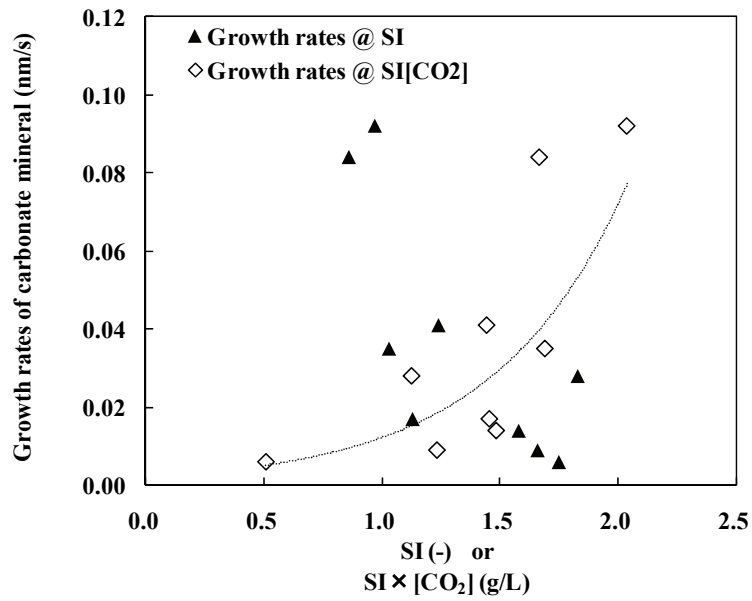
Fig. 3.24: Correlation with S.I x [CO_2] and growth rates of carbonates for the in-situ test at Ogachi HDR site.
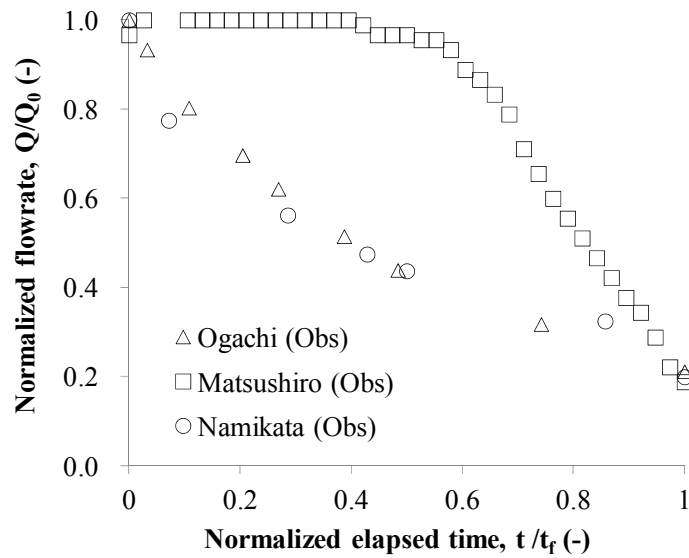
Fig. 3.25: Comparison of all cases of discharge flow rate curves.

Dissolved reactants including CO_2 might affect the dissolution rate of plagioclase and granite, the reaction behavior has been suggested recently in several studies (Sorai et al., 2007; Suto et al., 2007). It is necessary that not only the high S.I. value but also the high concentration of chemical reactants (Ca and CO_2) would be considered as a contribution to the precipitation of $CaCO_3$. In this study, the product of S.I. and CO_2 concentration (S.I. x $[CO_2]$) as another index is more suitable than S.I. to evaluate the possibility of carbonate precipitation focused on CO_2 concentration in solution. When fluid contains a large amount of reactants even if S.I. is relatively low, a large amount of carbonate mineral is likely to precipitate in porous media. The large order of S.I. x $[CO_2]$ indicates Matsushiro, Ogachi and Namikata consequently. This result agreed well with the order of required clogging time which was defined as duration by when the flow rate declined up to about 20 % of the initial flow rate. Therefore, not only S.I. but also concentration of reactants should be considered in order to clear the clogging mechanism of carbonate mineral precipitation.

Fig. 3.25 showed that carbonates deposited over the entire column due to high fluid velocity for the Matsushiro case. Flow rate decreased after about a day since flow path might be clogged up with carbonates. In contrast, for the Namikata and Ogachi case, flow rate decreased immediately at the beginning of the experiment as precipitation is concentrated at the inlet. These results provided that the distribution of the amount deposits governed by the fluid velocity (Fig. 3.11) affect the flow rate curves. Hence, numerical analysis for clogging models should be taken account of advection-precipitation phenomena.

CHAPTER 4   NUMERICAL ANALYSIS FOR CLOGGING MODELS

4.1   Introduction

This chapter aims to simulate the one-dimensional flow experiments based on the results of clogging at field and laboratory scaled tests. Advection-precipitation model adopted one-dimensional flow in a single fracture and in porous media. A step-wise numerical calculation method was developed to provide predictions of when and where carbonate deposits might be found through reservoirs during carbon dioxide (CO_2) sequestration. Flow experiments through porous media using a supersaturated carbonate fluid were performed in order to observe flow rates. At constant differential total head, permeability reduction was measured by a decrease in flow rates. In order to evaluate precipitation rates and permeability change in the formation, calculated flow rates based on the proposed geochemical clogging model were compared with the experimentally observed data. Both high and low temperature cases were studied to understand how hydrothermal conditions can affect precipitation rates of carbonate. According to chemical kinetics, growth rates of mineral are generally proportional to saturation index (S.I.) that depends on temperature. Thus, supersaturated fluid has an advantage of improving the filtration and the amount of carbon fixation (σ). However, when the ratio of filtration coefficient (λ) to pore fluid velocity (u) increases, the permeability around the injection point tends to be significantly reduced by carbonate accumulation, and thus, this might result in insufficient injection of CO_2. Therefore, it is essential to understand how to control both λ and u so that the precipitation of carbonate can be located as far away from the inlet as possible.

4.2   Theoretical backgrounds

4.2.1   Advection-reaction equation

As is well known, the calcite deposits are represented as two-component system of Ca^{2+} and CO_3^{2-} in Eq.(4.1).

$$CaCO_3 = Ca^{2+} + CO_3^{2-} \tag{4.1}$$

The rate of calcite precipitation is regulated by both changes in Ca^{2+} and CO_3^{2-} concentration in the fluid. HCO_3^- is a main species in neutral pH. We calculated the equilibrium conditions in Eq.(4.1), which also thermodynamically represents the real reaction. For this reason, the precipitation rate is replaced as a one-component fluid with Ca^{2+} for convenience. When concentration of Ca is less than that of CO_3 for example in the case of Namikata, amount of deposited Ca might be overestimated.

In this calculation, the conservation of mass for one-dimensional transport with calcite deposition process in porous media (Fig. 4.1) is modeled by an advection-reaction formulation as Eq.(4.2) (Parkhurst and Appelo, 1999; Shikazono et al., 2009):
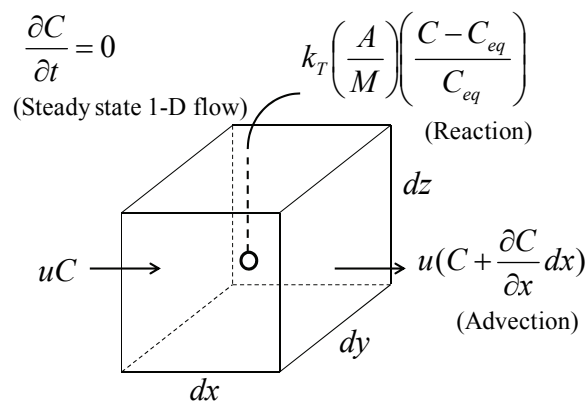
Fig. 4.1: Conservation of mass for the advection-reaction in one-dimensional flow.

$$\frac{\partial C}{\partial t} = -u \frac{\partial C}{\partial x} - k_T \left(\frac{A}{M} \right) \left(\frac{C - C_{eq}}{C_{eq}} \right)$$

(4.2)

where C is the Ca^{2+} concentration in flowing water (g/cm^3), C_{eq} is the equilibrium Ca^{2+} concentration in water (g/cm^3), which is temperature dependent, t is time (s), u is the fluid velocity in porous media (cm/s), x is distance (cm), A/M is the specific reactive surface area (A) per kg of H_2O (M), and k_T (mol· cm^{-2}· s^{-1}) is the rate constant of the chemical reaction at T, which can be shown as a function of temperature by Arrhenius Eq.(4.3):

$$k_T = k_{25} \exp \left[\frac{-E_a}{R} \left(\frac{1}{T} - \frac{1}{298.15} \right) \right]$$

(4.3)

where E_a is the activation energy, R is the gas constant, T is the absolute temperature, and k_{25} is the rate constant at 298.15 K.

In the case of steady state flow when concentrations of Ca^{2+} and CO_3^{2-} are constant, the general solution of Eq.(4.2) can be described by Eq.(4.4) when the concentration at the inlet ($x=0$) equals the influent concentration (C_i'):

$$C' = C_i' \exp \left[- \left(\frac{k_T A}{C_{eq} M} \right) \left(\frac{x}{u} \right) \right]$$

(4.4)

where C' ($=C-C_{eq}$) is the supersaturated concentration if S.I. > 0. Introducing the filtration coefficient (λ) defined as $\lambda=(k_T/C_{eq})$· (A/M), Eq.(4.4) can be rewritten by Eq.(4.5).

$$C' = C_i' \exp \left[-\frac{\lambda}{u} x \right]$$

(4.5)

The solubility product ($K_{sp}=a(Ca^{2+})a(CO_3^{2-})$) constant for calcite in geothermal fluid is a function of temperature, as shown in Eq.(4.6) (Arnórsson et al., 1982).

$$K_{sp} = 10.22 - 0.0349\,T - 2476\,/\,T \qquad\qquad (\,4.6\,)$$

The concentration of Ca^{2+} is assumed to be nearly equal to that of CO_3^{2-}, and the equilibrium concentration of Ca^{2+} can be calculated by Eq.(4.7).

$$C_{eq} = \sqrt{K_{sp}} = \sqrt{10.22 - 0.0349T - 2476/T} \qquad\qquad (\,4.7\,)$$

Finally, temperature dependent precipitation rates of calcite (v_n) defined as $v_n = k_T/C_{eq}$ become Eq.(4.8).

$$v_n = \frac{k_{25}\exp\!\left[\dfrac{-E_a}{R}\left(\dfrac{1}{T} - \dfrac{1}{298.15}\right)\right]}{\sqrt{10.22 - 0.0349T - 2476/T}} \qquad\qquad (\,4.8\,)$$

This calcite precipitation causes the fluid flow to clog in porous media and the aim of our study is to investigate change of the precipitation rates by flow conditions. In two experiments, both mentioned above, we had observed that the clogging decreases the permeability of porous media and leads to reducing amounts of flow. From Eq.(4.8) the precipitation of calcite is controlled by not only the rate constant of the chemical reaction (k_{25}) but also temperature (T). Therefore the various range of temperature can be considered by Eq.(4.8). The estimation method of k_{25} values from observed data sets will be proposed in the following sections.

4.2.2   Evaluation of filtration coefficient

Fig. 4.2 illustrates three mechanisms that can explain particle migration with the filtration theory. Particles large enough to retard the penetration can form a filter cake at the face of the media. As a result, substantial particle accumulation can occur, leading to a decrease in permeability. For particles smaller than the porous media grain size, penetration into the media will occur. Precipitated particles can be mechanically removed by straining in pore spaces. However, capacity of pore spaces for particle accumulation will be limited because straining near the face of porous media significantly restricts openings, allowing smaller particles to be retained in a filter cake. Filtration of most concern with regard to size of pore and migrating particle is effective to evaluate clogging phenomena.

In column tests performed at Matsushiro and Namikata site, carbonate crystal were already formed in the carbonated solution. In this case, the process of adsorption and accumulation on the surface of the porous media was shown as Fig. 4.2 (a) and (b). On the other hand, the column test results at high temperature in Ogachi site, carbonate crystal was dissolved in the solution before injecting into the column. Precipitation of carbonate mineral occurred inside the column under supersaturated condition due to high temperature. The solubility of carbonate mineral is lower at higher temperature and vise versa in contradiction to silicate minerals. As shown in Fig. 4.2 (c), carbonate minerals in supersaturated condition may grow from a species of carbonate mineral once it has formed on the rock surface.

(a) Filter cake   (b) Straining   (c) Physico-chemical precipitation
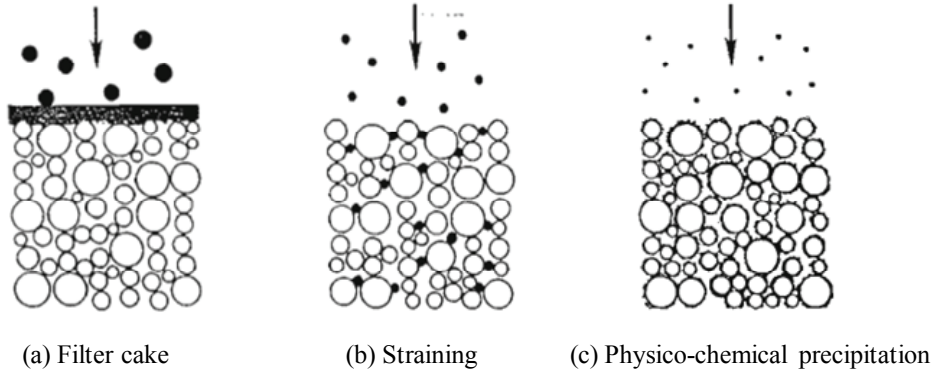
Fig. 4.2: Particle size dependence in the three filtration mechanisms (after McDowell-Boyer et al., 1986).

Filtration coefficient (λ), which means an ability of a particle capture to collect on the surface of media, can examine two different approaches for evaluating λ. The first one is a particle capture probability approach adopted by Reddi and Bonala (1997). For a filter whose pore-size distribution can be characterized by a log-normal distribution, they obtained

$$\lambda = \frac{u}{\alpha^* e^{2(b^2+m)}}\left[4K_1 - 4K_2 e^{(b^2-2m)/2} + K_3 e^{2(b^2-m)}\right] \qquad (4.9)$$

where $K_1=(3a)^2$, $K_2=(3a)^3$, $K_3=(3a)^4$, a = size of the migrating particle, α^* = characteristic length of pores and taken as 9.11 mm for coarse-grained soils, and m, b = the mean and standard deviation of the log-normal pore size distribution of the filter. λ is a function of the pore fluid velocity (u), pore size (α^*) and its distribution (m, b) and size of migrating particles (a). But this approach has difficulties for determining the precise parameters in micro scale for carbonate fluid flow experiments.

The second approach is based on estimation with experimental results, as described by Gruesbeck and Collins (1982). When a particulate suspension is fed to a filter soil column of length L, steady state concentrations can be observed at a specific

effluent concentration C_e. Substituting $C'= C_i$ at $x=0$ and $C'= C_e$ at $x= L$ into the Eq.(4.4), λ can be derived as:

$$\lambda = \frac{u}{L} \ln \frac{C_i}{C_e}$$

(4.10)

where C_i = particle concentration in the influent, λ can be determined using all the known quantities on the right-hand side of Eq.(4.10).

For the our fluid flow experiments in in-situ and laboratory scale, evaluation of λ using Eq.(4.10) is reasonable because this approach meets the physical and chemical characteristics of the pore fluid and porous media. Eq.(4.10) is equivalent to Eq.(4.11) determined from Eq.(4.4).

$$\lambda = \frac{k_T}{C_{eq}} \left(\rho_w \frac{A}{M} \right)$$

(4.11)

λ is a function of the rate constant of the chemical reaction at T (k_T), the equilibrium Ca^{2+} concentration in water (C_{eq}) , the specific reactive surface area per kg of H_2O (A/M) and ρ_w (g/cm^3) is density of water at T.

The geochemical reactions should be considered for a detailed prediction of the time scales in CO_2 fixation by using both equilibrium and kinetic approach. There is a key to obtain reaction rate data of high accuracy. Database of thermodynamics parameters are summarized in many species about pH dependence of dissolution rate constant, reaction order and activation energy by Palandri and Kharaka (2004).

In real conditions, λ is cannot be constant in this advection-reaction process because filtration ability will vary with the concentration of chemical compositions in carbonate suspensions and with the properties of the porous media. As shown in equation

Eq.(4.12), λ can be also expressed simply as the product of two factors, the precipitation rate (v_n,$=k_T/C_{eq}$, [cm/s]) and the specific reactive surface area ($S=\rho_w A/M$, [cm^2/cm^3]).

$$\lambda = v_n S \qquad\qquad\qquad (4.12)$$

4.3   Numerical modelling methods

A series of flow experiments have been carried out under different temperature conditions to verify that the developed numerical methods is available to provide sealing information based on theory of fluid mechanics and geochemistry. A step-wise numerical calculation was programmed by spread sheet for the clogging model in two models taken into account for physical and physical-chemical (geochemical) properties as shown in Fig. 4.3. A flow rate curve calculated by a porous media model was matching to one observed in a column test. A permeability curve calculated by a fracture media model was fitting to one observed in in-situ test. These curve fitting was performed to predict and validate carbonate precipitation phenomena.
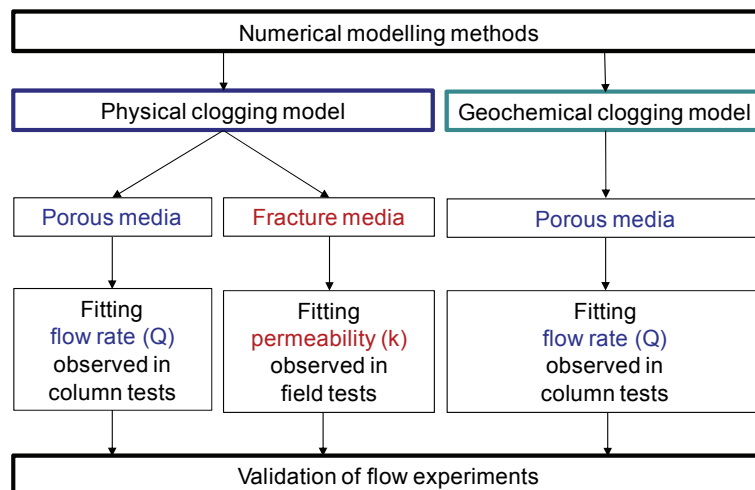
Fig. 4.3: Schematic flow chart for numerical modelling methods.

4.3.1   Physical clogging model

Assuming constant precipitation rates with time, physical clogging model is able to reproduce the permeability change in rock pore and rock fracture (Fig. 4.4). While the porous media model is applicable to column tests which give flow rates with porosity change, the fracture model is available for in-situ tests, which are dominant in aperture change in fractured media, to compare with observed and calculated permeability.

Porous media model

In this model, the decrease of porosity results from the calcite deposition as Eq.(4.13)

Start

Read test dimensions and properties

Precipitation rate, v_n=constant

Porosity, $n=n_o-((r+v_nt)^3-r^3)/r^3$

Deferential head, $\Delta h(t)$

Hydraulic gradient, $i(t) =\Delta h(t)/L$

Permeability, $k(t)$
from Kozeny-Carman equation

Pore velocity, $u(t)=k(t)i(t)/n(t)$

Flow rate, $Q(t)=k(t)i(t)A$

$t>t_{max}$

No

$t=t+\Delta t$

Yes

Print out

Stop

(a)

Start

Read test dimensions and properties

Initial aperture of a single fracture, b_o

Aperture of a fracture, $b(t)$

Pore velocity, $u(t)$

Following Cubic law,
Flow rate, $Q(t)$

Precipitation rate, v_n=constant

$b(t+\Delta t)=b(t)-v_n\Delta t$

Permeability around the borehole, $k(t)$

$b(t+\Delta t)<0$

No

$t=t+\Delta t$

Yes

Print out

Stop

(b)

Fig. 4.4: Calculation procedure of physical clogging models.
(a) Porous media model (b) Fracture model

$$n(t) = n_0 - \frac{(r + v_n t)^3 - r^3}{r^3} \tag{4.13}$$

where n = porosity; n_0 = initial porosity; r = radius of a porous material; and v_n = precipitation rate. Carbonated water flows perpendicular to the cross section of column in one-dimensional flow. The relative permeability (k/k_0), where k_0 is the initial permeability, shows porosity (n)-permeability (k) relationship for spherical grain model as Eq.(4.14) following Kozeny-Carman equation (Carrier, 2003):

$$\frac{k(t)}{k_0} = \left(\frac{n}{n_0}\right)^3 \left(\frac{1 - n_0}{1 - n}\right)^2 \tag{4.14}$$

Fracture model

When the fluid flow is steady and isothermal, the flow rate, $q(t)$ can be written in a simplified equation which is called "cubic law" for flow in an "open" fracture; i.e., the planar surfaces remain parallel and thus are not in contact at any point (Witherspoon et al., 1979). By summing flow rates of total fractures, flow rate through rock mass is available to express as Eq.(4.15)

$$q(t) = \frac{N g b(t)^3}{12 v} i \tag{4.15}$$

where $b(t)$ = the aperture of fracture at t; g = gravity acceleration; v = the kinematic viscosity; N = number of the fractures intersecting the injection hole; and i = hydraulic gradient. In the developed model, permeability or porosity changes with deposition in fractures. Following the laminar flow in parallel planar plates to represent the fracture surfaces, permeability of a fracture at t, $k_f(t)$ is given by Eq.(4.16) with an aperture, $b(t)$.

$$k_f(t) = \frac{gb(t)^2}{12\nu}$$ (4.16)

Average permeability including entire fractures is as shown in Eq.(4.17):

$$k(t) = \frac{N\widetilde{b}}{L} k_f(t)$$ (4.17)

where L = length of a bore hole at test section; and $\widetilde{b}$ = average aperture equivalent to an initial aperture, b_0. Substituting Eq.(4.16) for Eq.(4.17), an initial aperture is shown in the following equation:

$$b_0 = \sqrt[3]{\frac{12L\nu k}{Ng}}$$ (4.18)

Pore velocity of fluid at t, $u(t)$ is given by Eq.(4.19).

$$u(t) = \frac{q(t)}{b(t)}$$ (4.19)

In this simulation, we assumed that precipitation rate is constant with time and equivalent to the initial precipitation rate, v_n.

$$b(t + \Delta t) = b(t) - v_n \Delta t$$ (4.20)

The change of flow rates, apertures and pore velocities at next time, $t+\Delta t$ are simulated by following such iteration until aperture becomes zero using Eq.(4.20).

4.3.2   Geochemical clogging model

Clogging model was applied for one-dimensional flow in porous media with constant differential total head and verified with a series of flow experiments. The amount of Ca ($\sigma_{i,j}$), flow rates ($Q_{i,j}$) and precipitation rates (v_n) can be evaluated assuming constant within a small discretized grid for computational purposes in each step following the procedure in Fig. 4.5. The subscripts i and j represent the space grid index and the time index, respectively.
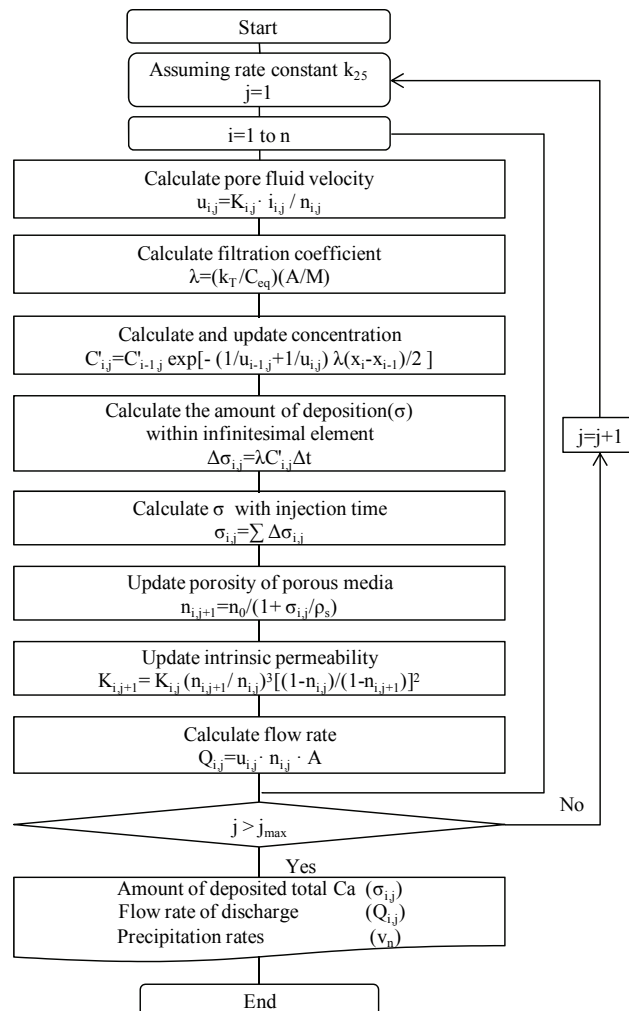
Fig. 4.5: Calculation procedure of geochemical clogging models on the porous media.

In the laboratory experiments, flow rates ($Q_{i,j}$) are monitored with elapsed time to predict precipitation rates (v_n). We adopted the trial-and-error approach in order to estimate k_{25} from obtained data sets; given appropriate initial k_{25} value, the various factors (e.g., pore fluid velocity ($u_{i,j}$), supersaturated concentration ($C'_{i,j}$), amount of deposited Ca ($\sigma_{i,j}$), porosity ($n_{i,j}$) and intrinsic permeability ($K_{i,j}$)) can be estimated step by step by using the computational procedure in Fig. 4.5. Applying Darcy's law to the column tests, the porosity-intrinsic permeability relationship is assumed to obey the Kozeny-Carman equation (Carrier, 2003). It is possible to obtain the change of flow rates with updated intrinsic permeability for a given rate constant k_{25}. The pore fluid velocity ($u_{i,j}$) can be expressed as Eq.(4.21):

$$u_{i,j} = K_{i,j} \cdot i_{i,j} / n_{i,j} \tag{4.21}$$

where $i_{i,j}$ is hydraulic gradient, $K_{i,j}$ and $n_{i,j}$ are intrinsic permeability and porosity of the porous media, respectively.

The geochemical clogging model adopted theses properties of porous media and fluid (Table 4.1) in order to reproduce flow experiments for the Ogachi, Matsushiro and Namikata cases. The initial intrinsic permeability ($K_{i,0}$) was calculated with the initial flow rates ($Q_{i,0}$). Although the concentration of Ca^{2+} exponentially decreases with the distance of fluid flow, we assumed that this value is constant within the infinitesimal grid elements. The supersaturated concentration in the zone between x_{i-1} and x_i during Δt can be expressed as Eq.(4.22):

$$C'_{i,j} = C'_{i-1,j} \exp\left[\frac{-\lambda(x_i - x_{i-1})}{2}\left(\frac{1}{u_{i-1,j}} + \frac{1}{u_{i,j}}\right)\right] \tag{4.22}$$

Table 4.1: Properties used for numerical calculation.

Properties for numerical calculation	Ogachi	Matsushiro	Namikata
Density of deposited Ca, ρ_s (g/cm^3)	1.55	1.55	1.55
Density of porous material, ρ_m (g/cm^3)	2.66	2.50	2.50
Density of fluid, ρ_f (g/cm^3)	0.882	0.989	0.998
Initial porosity, n_0 (-)	0.27	0.39	0.29
Initial flow rate, Q_0 (cm^3/s)	5.5	17.7	13.3
Initial intrinsic permeability, K_0 (cm/s)	0.44	0.39	0.27
Specific reactive surface area, A/M (cm^2/g)	9.8	9.8	9.8
Specific reactive surface area, $S(=\rho_f (A/M))$ (cm^{-1})	8.64	9.69	9.78
Unit distance, Δx (cm)	1	0.8	1
Differential time, Δt (s)	60	23	360
Total head of inlet, h_0 (cm)	50	42	100
Total head of outlet, h_L (cm)	0	0	0
Hydraulic gradient, i (-)	1	1.05	2
Initial concentration of Ca^{2+}, C_i (g/cm^3)	2.8×10^{-4}	8.5×10^{-4}	1.8×10^{-5}
Equilibrium concentration of Ca^{2+}, C_{eq} (g/cm^3)	2.6×10^{-7}	4.4×10^{-6}	5.9×10^{-6}
Supersaturated concentration of Ca^{2+}, C_i' (=C_i-C_{eq}) (g/cm^3)	2.8×10^{-4}	8.5×10^{-4}	1.2×10^{-5}
Temperature of fluid, T (°C)	185	49.0	20.2
Activation energy, E_a (kJ/mol)	41.87	41.87	41.87
Rate constant at 25°C, k_{25} (mol/m^2/s)	1.0×10^{-10}	9.5×10^{-11}	3.0×10^{-5}
Rate constant at T°C, k_T (mol/m^2/s)	3.7×10^{-8}	3.3×10^{-10}	2.3×10^{-5}
Precipitation rate of calcite, v_n (=k_T/C_{eq}) (cm/s)	1.2×10^{-3}	7.6×10^{-7}	3.9×10^{-2}
Filtration coefficient, λ (s^{-1})	0.011	7.3×10^{-6}	0.38

Precipitation reaction is described as the first-order rate law by previous filtration studies (Ives, 1975; Gruesbeck and Collins, 1982; Kim et al., 2009) as Eq.(4.23):

$$\frac{\partial \sigma_{i,j}}{\partial t} = \lambda C'_{i,j}$$

(4.23)

Then, the total amount of deposited Ca is expressed as the cumulative amount of deposits in Eq.(4.24).

$$\sigma_{i,j} = \sum_{j=1}^{j} \Delta \sigma_{i,j} = \sum_{j=1}^{j} \lambda C'_{i,j} \Delta t$$

(4.24)

This deposited Ca changes the porosity. The porosity at position i and time step $j+1$ is updated by Eq.(4.25):

$$n_{i,j+1} = n_0 - \frac{n_{i,j} \sigma_{i,j}}{\rho_s}$$

(4.25)

which can be simplified as Eq.(4.26) when assuming $n_{i,j}$ is approximately equal to $n_{i,j+1}$:

$$n_{i,j+1} = \frac{n_0}{1 + \sigma_{i,j} / \rho_s}$$

(4.26)

where n_0 is the initial porosity and ρ_s is the density of Ca.

$Q_{s,i,j}$ means the deposits mass ratio defined by the mass of carbonate mineral per unit mass of filter as shown in Eq.(4.27).

$$Q_{si,j} = \frac{n_{i,j} \sigma_{i,j}}{\rho_m (1 - n_0)}$$

(4.27)

By multiplying ($1+\alpha Q_{si,j}$), Eq.(4.27) can be rewritten in the following equation:

$$\lambda_{i,j} = v_n S (1 + \alpha Q_{S,i,j}) \tag{4.28}$$

where α is non-dimensional acceleration coefficient with carbonate precipitation and $\alpha=0$ means no effect of accelerating deposition rates. α applied to this model since λ is not always constant for the filtration phenomena. In reality, the effect of extending the reactive surface area might be accelerated by attachment of carbonate precipitation on the porous media. For calcite, required specific reactive surface area (A/M) and activation energy (E_a) are respectively given as 9.8 cm^2/g and 41.87 kJ/mol in Table 4.1 (Xu et al., 2004b).

Based on the Kozeny-Carman equation with porosity change, the intrinsic permeability at time step $j+1$ is updated as Eq.(4.29) at all space grid points i:

$$K_{i,j+1} = K_{i,j} \left(\frac{n_{i,j+1}}{n_{i,j}}\right)^3 \left(\frac{1-n_{i,j}}{1-n_{i,j+1}}\right)^2 \tag{4.29}$$

Decrease of pore fluid velocity caused by calcite precipitation accounts for the reduction of flow rates. Finally, the calculated flow rates, as per Eq.(3.30), can be matched to observed data in column tests in order to evaluate precipitation rates:

$$Q_{i,j} = u_{i,j} \cdot n_{i,j} \cdot A \tag{4.30}$$

where A is the cross-sectional area of the column packed with porous media. If observed and calculated flow rates have a large discrepancy, the rate constant (k_{25}) assumed initially is modified until both flow rates become close enough.

4.4   Results and discussion

4.4.1   Physical clogging model

While the fractured hydrothermal reservoir consists of fracture, the lab-scaled experiments are dominated by the characteristic of porous media. The flow results from field and lab-scaled experiments at the Ogachi HDR site show the differences in the clogging mechanisms under the condition of constant flow rate and under the condition of constant head, respectively. These results are due to the fact that the initial pore fluid velocity of in-situ test was more than 100 times higher than that of the column test. Once transported and settled in pores, constant head conditions cause deposited particles to remain on the porous media. Under constant flow rate conditions, however, they might become detached and re-entrained downstream due to increased pore fluid velocity (Reddi et al., 2005, 2010).

Porous media model

For the column experiments (at Ogachi, Matsushiro and Namikata), the porous media type of physical clogging models was applied to three types of carbonate fluids under constant head. Flow rate was calculated to compare with observed one, as shown in Fig. 4.6. This porous media type evaluated precipitation rates as 0.13nm/s, 0.01nm/s, 0.037nm/s in the cases of high temperature, high concentration of CO_2, and high pH, respectively. As shown in Fig. 4.6 (b), it is difficult for high concentration type to fit flow rate curves because the high fluid pore velocity governs uniform distribution of deposited carbonate amounts.
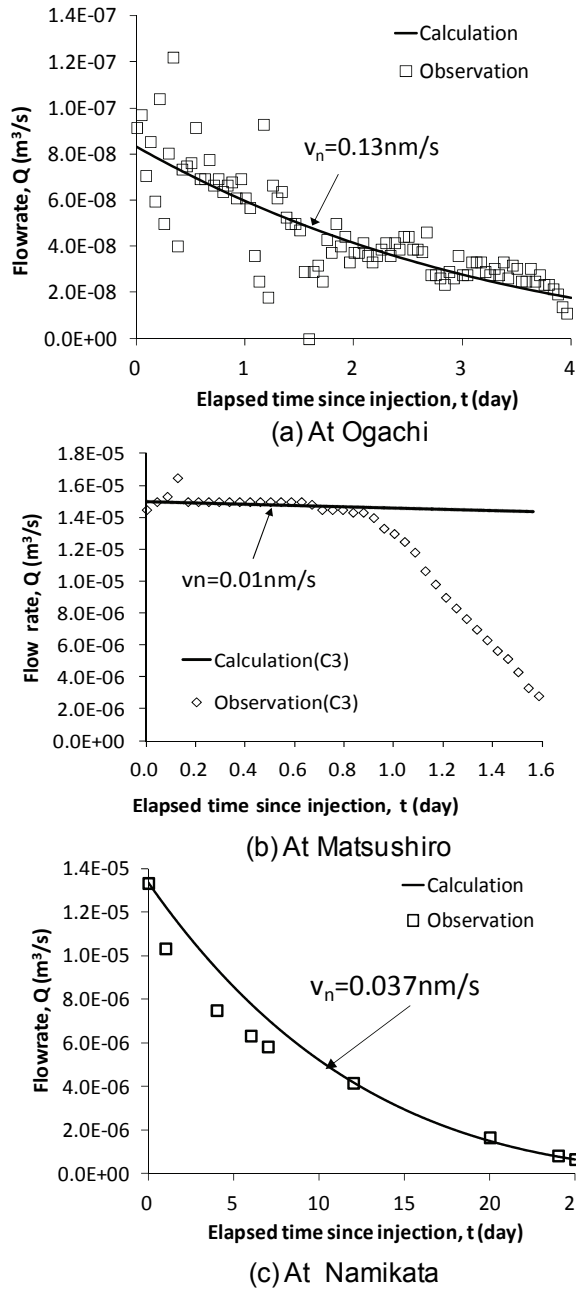
(a) At Ogachi

(b) At Matsushiro

(c) At Namikata

Fig. 4.6: Evaluation of precipitation rates by a curve fitting in the column experiments.
(a) High temperature type (b) High concentration type (c) High pH type

Fracture model

In the field experiment, flow rates into the bore hole were kept constant in each cycle and differential head was measured between shut-in and re-injection. The field tests showed difficulty in measuring discharge flow rates in reservoirs. In place of flow rates, the intrinsic permeability was obtained through the groundwater level changes. The intrinsic permeability calculated by Eq.(4.17) was fitted with the one observed by Eq.(3.2), as shown in Fig. 4.7. The discrepancies in gradients of the fitting curve are shown between initial and final phase beginning approximately two days after injection. According to results, precipitation rates may depend on time. When the fracture type of physical clogging models is fitted to the permeability which is derived from the in-situ test through fracture media at the initial stage, the precipitation rate is 3.5×10^{-3} nm/s. However, the precipitation rate decreases by about one-third (= 1.0×10^{-3} nm/s) after two days.
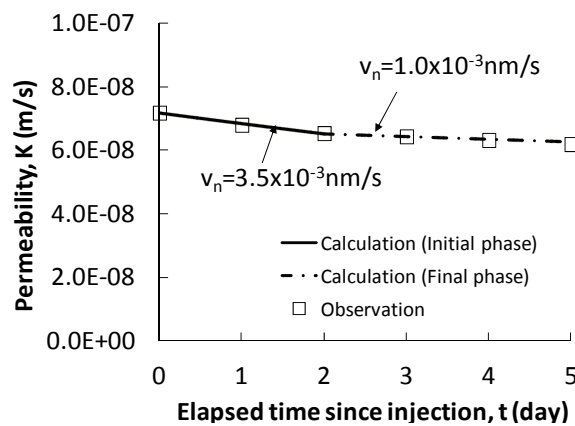
Fig. 4.7: Evaluation of precipitation rates by a curve fitting in the field experiment.

4.4.2   Geochemical clogging model with acceleration coefficient

The curve fitting method was applied to this model by comparing calculated value with those observed from flow experiments. As shown in Fig. 3.19, numerical calculation was carried out from Stage 2 to Stage 3 with input data in Table 4.1. A physical clogging model provides a gradual drop in flow rates (Fig. 4.8 (a)), as constant precipitation rates result in the linear decline of porosity and permeability as shown in Fig. 4.8 (b).
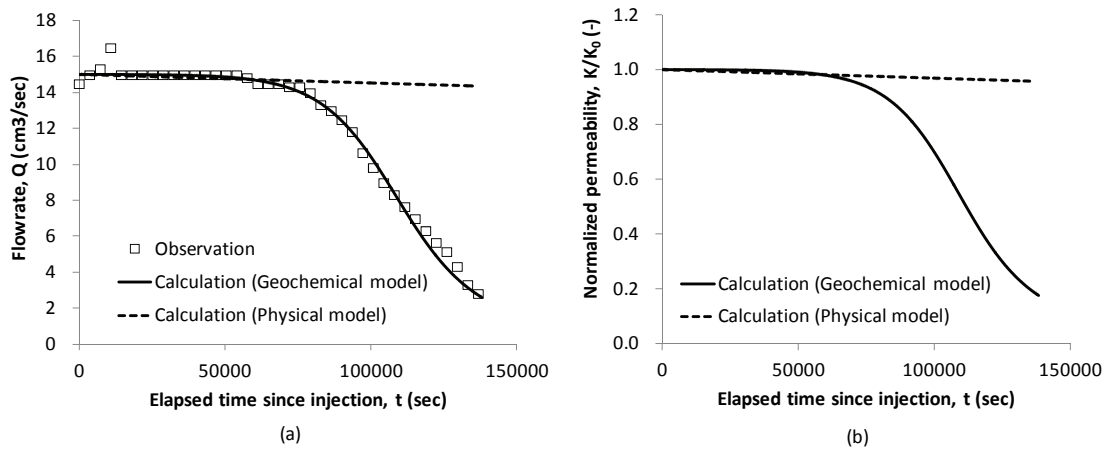
Fig. 4.8: Comparison of results in geochemical and physical clogging models for case 3.
(a) Flow rate (b) Normalized permeability

Table 4.2: Calculation results using a geochemical clogging model.

Case	Pore fluid velocity, u (cm/s)	Amount of precipitation, σ (g/cm^3)	Acceleration coefficient, α (-)	Precipitation rates, v_n (nm/s)
C1	6.41 (Initial stage) 1.37 (Final stage)	1.70	250	796
C2	7.74 (Initial stage) 1.92 (Final stage)	1.70	48000	8.0
C3	5.44 (Initial stage) 1.73 (Final stage)	1.28	48000	7.6

Meanwhile, the geochemical model provides an enlargement in filtration coefficient (λ) with an increase in the specific reactive surface area (S) covered with the carbonate layers, as shown in SEM images (Fig. 3.18). The acceleration coefficient (α) with carbonate deposits in Eq.(4.28) was determined appropriately to fit the flow rate curves for the Matsushiro column tests (Fig. 4.9 (a)); common results from three cases are found below.

1. The head loss in the porous media increases with time (Fig. 4.9 (b)) as a result of particle accumulation (Fig. 4.9 (d)).

2. A minimum porosity with carbonates accumulation (Fig. 4.9 (e)) results in the maximum pore fluid velocity near the inlet (Fig. 4.9 (c)).

3. The decrease of supersaturated concentration of Ca (Fig. 4.9 (f)) may account for the filtration of carbonate particles in the porous media.

Each amount of precipitation in cases C1, C2 and C3 indicate 1.70, 1.70, and 1.28 g/cm^3 respectively. By comparing C2 and C3, the precipitation rate for the C2 case is slightly larger than one for the C3 case due to a larger differential total head. The precipitation rate for the C1 case is the fastest due to the sterilization process. This result is consistent with the large difference in precipitation rates observed in experiments with glass plates between a drainage and discharge of column. Fe ion concentration may decrease relatively because hot spring fluid in the drainage was exposed to air causing Fe(OH)$_3$ to precipitate.
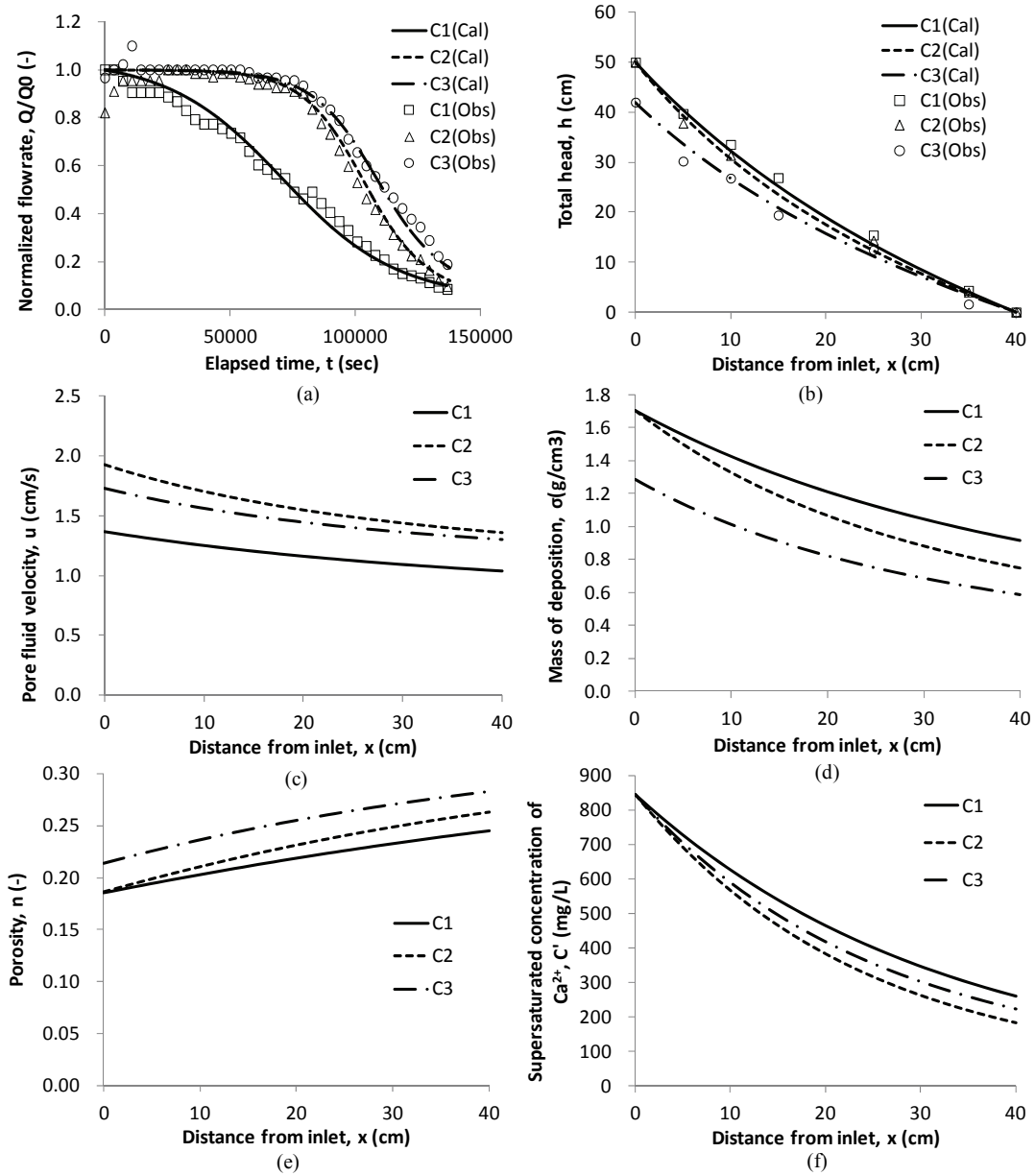
Fig. 4.9: Results of the geochemical clogging model for the Matsushiro cases.
(a) Flow rate (b) Total head (c) Pore fluid velocity
(d) Mass of deposition (e) Porosity (f) Supersaturated concentration of Ca^{2+}

4.4.3   Comparison of results using the geochemical clogging model

The proposed clogging model can predict the change of fluid and porous material characteristics with respect to both injection time and space grid points. In all cases, a comparison of results (Fig. 4.10, Fig. 4.11, Fig. 4.12) provides insight into the best conditions for mineral trapping.

Precipitation rates are determined from the gradient of the flow rate curve during the beginning stage (Fig. 4.13 (a)). The steeper the gradients, the larger the precipitation rates. For the Matsushiro case, the precipitation rate is the lowest in three cases. After a day, the flow rate began to decrease by about 10% because deposits of carbonate particles on the glass beads gradually enlarged the apparent reactive surface area.

In addition, λ/u is a key parameter in helping us understand the distribution of carbonate mineral precipitation. The smaller the λ/u, the more uniform the amount of deposited carbonates, as illustrated in the cases of Ogachi and Matsushiro. The carbonate fluid at Ogachi and Matsushiro showed neutral pH, so high temperature affects precipitation rates easily. For this reason, precipitation rates in high temperature conditions (e.g. the Ogachi case) are much higher than those at lower temperature conditions (e.g. the Matsushiro case), as shown in Table 3.4. The precipitation rates generally are proportional to the initial filtration coefficients.

For the Matsushiro case, the calculated λ was increasing due to the extending reaction surface area; filtration improved dramatically upon injection of carbonate fluid. For the Namikata case, on the other hand, high pH(=11) fluid resulted in the largest filtration coefficient (λ) in all cases with a large rate constant (k_T). Therefore, distribution of deposited carbonates (Fig. 4.13 (b)) is likely to decline drastically. Observed images through SEM analysis (Fig. 3.22) aligned well with the calculations.
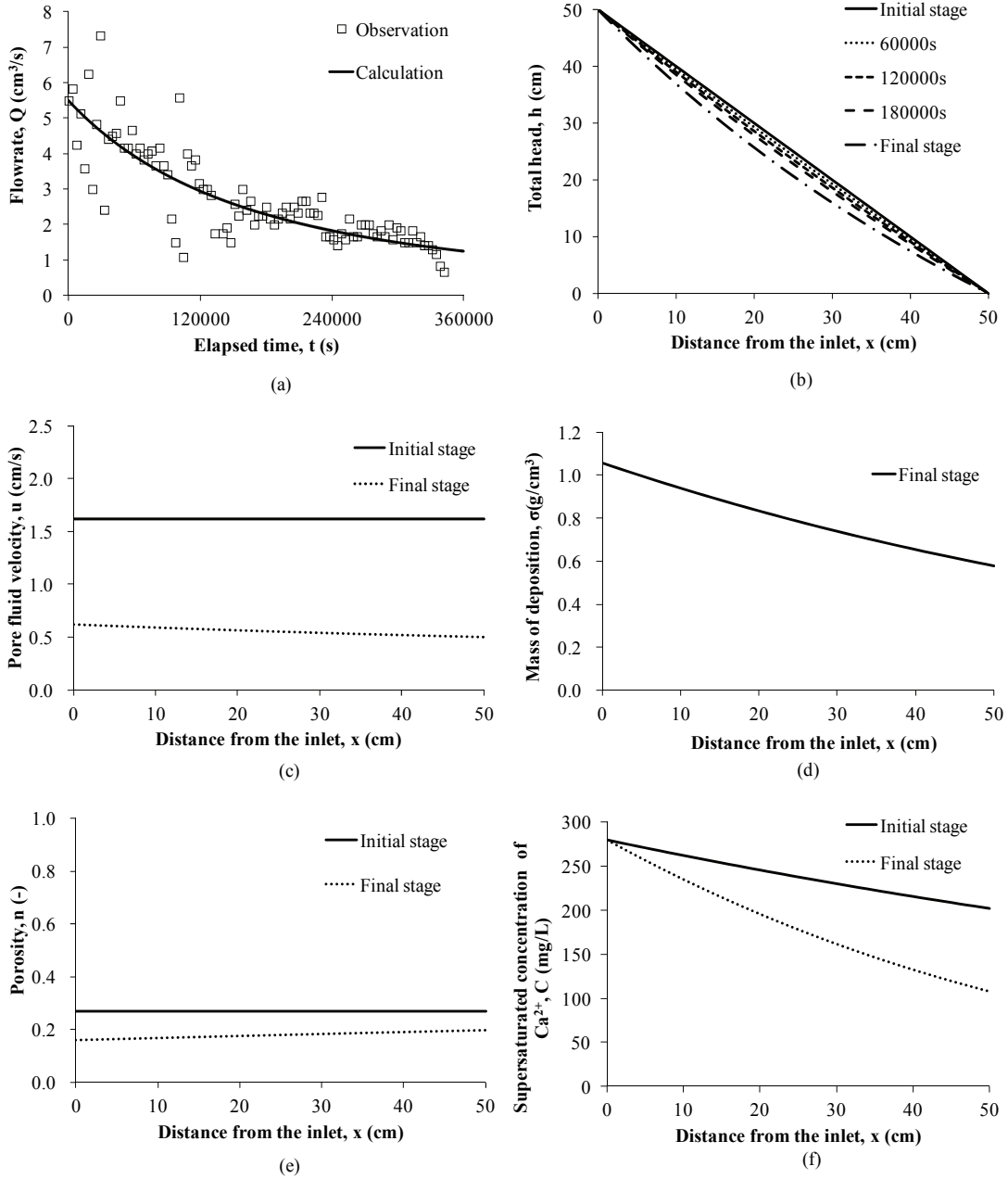
Fig. 4.10: Results of the geochemical clogging model for the high temperature
(T=185 °C). (a) Flow rate (b) Total head (c) Pore fluid velocity
(d) Mass of deposition (e) Porosity (f) Supersaturated concentration of Ca^{2+}

Fig. 4.11: Results of the geochemical clogging model for the high concentration
([CO$_2$]=1800mg/L). (a) Flow rate (b) Total head (c) Pore fluid velocity
(d) Mass of deposition (e) Porosity (f) Supersaturated concentration of Ca^{2+}
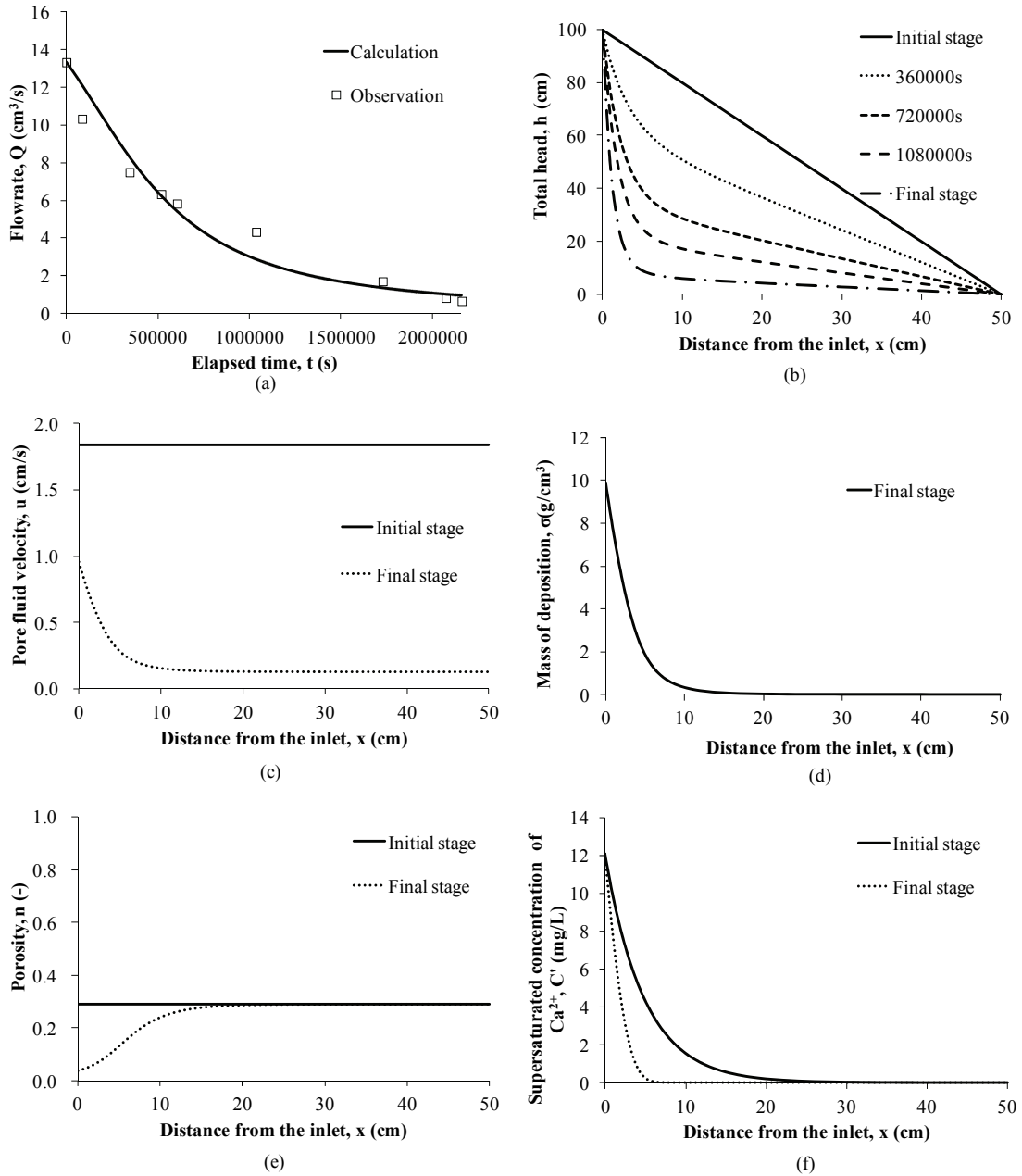
Fig. 4.12: Results of the geochemical clogging model for the high pH (pH=11).
(a) Flow rate (b) Total head (c) Pore fluid velocity
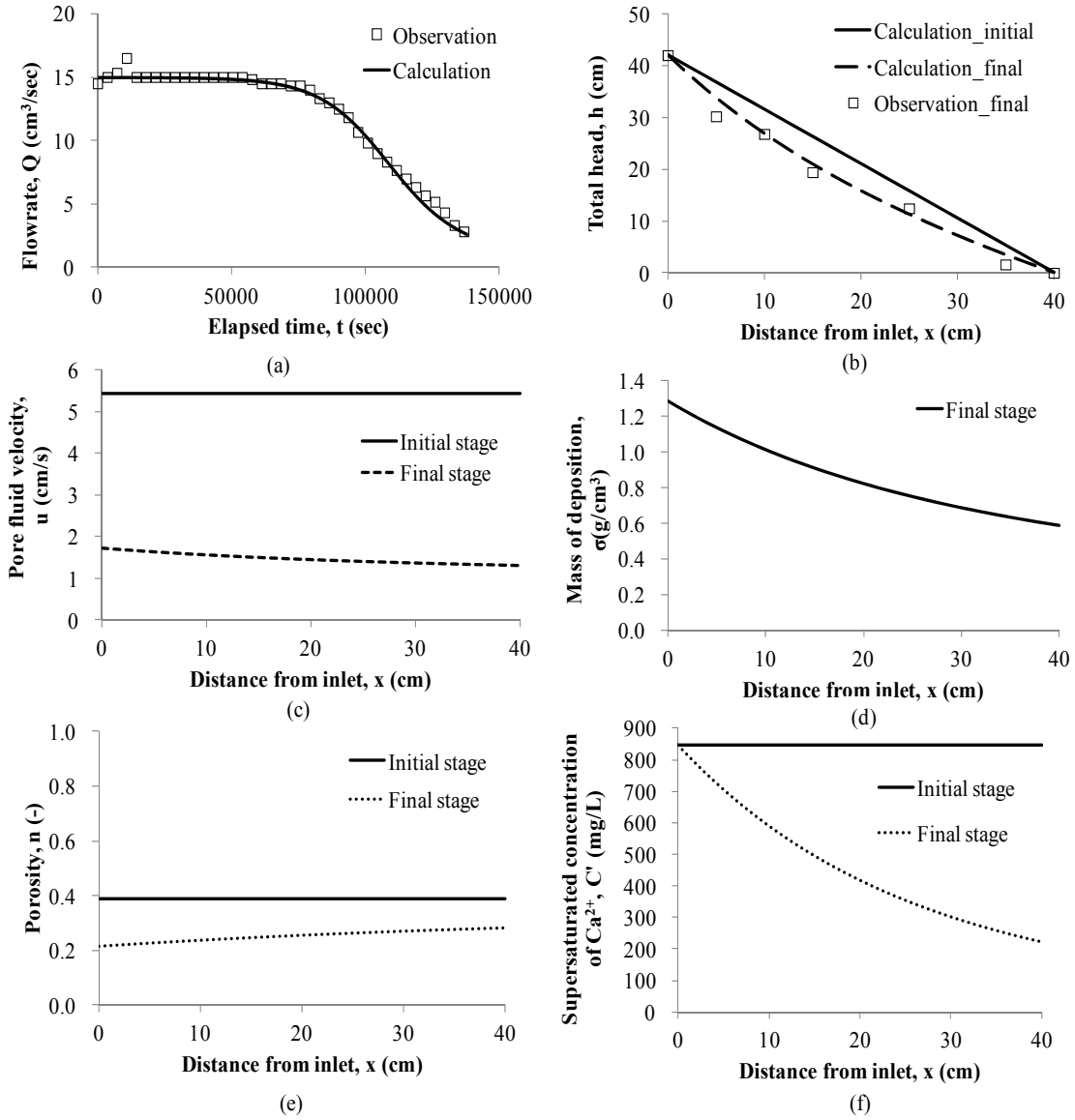(d) Mass of deposition (e) Porosity (f) Supersaturated concentration of Ca^{2+}

(a)

(b)
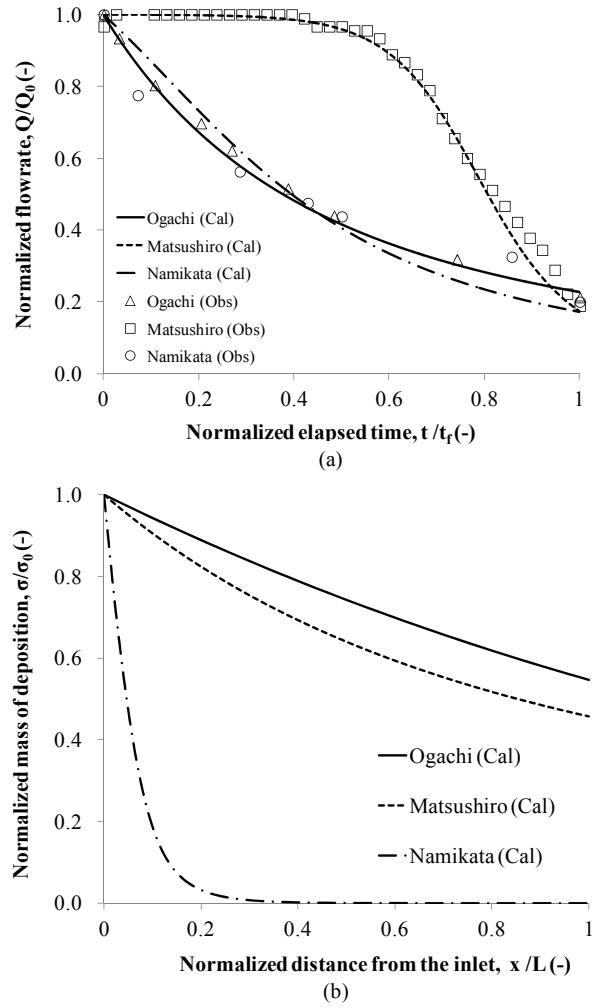
Fig. 4.13: Comparison of results using the geochemical clogging model.
(a) Normalized flow rate (b) Normalized mass of deposition

Table 4.3: Estimated filtration coefficient (λ) and precipitation rates (v_n).

Site	Filtration coefficient, λ (s^{-1})	The ratio of filtration coefficient to pore fluid velocity, λ/u (cm^{-1})	Precipitation rates, v_n (μm/s)
Ogachi	1.1×10^{-2}	1.70×10^{-2}	12.2
Matsushiro	7.3×10^{-6} (Initial stage) 6.3×10^{-2} (Final stage)	1.35×10^{-6} (Initial stage) 3.66×10^{-2} (Final stage)	7.56×10^{-3}
Namikata	0.38	0.395	386

4.5   Conclusions

A step-wised numerical analysis for clogging models in both physical and chemical aspects has focused on evaluating when and where precipitation of carbonates could be an advantage or a problem. A physical clogging model provided permeability change with respect to injection time. A physico-chemical clogging model was extended to provide predictions of when and where carbonate deposits might be found in reservoirs during carbonate fluid injection.

The results of developed numerical models indicate that dissolved CO_2 can be fixed as carbonate in the range of various temperatures, including both high and low temperatures. In this respect, several applications, such as geothermal power plants and the facility for propane storage, are favorable; quick mineralization may contribute to industrial applications for storage safety. Even if the Namikata case might be inappropriate for CO_2 sequestration due to scale problems around the borehole, the carbonate mechanism at low temperature is worth comparing to the neutral mechanism (pH= 6~7) for the Ogachi and Matsushiro case, if only as a modeling validation exercise.

With respect to distance, the amount of precipitation is distributed rather uniformly in Ogachi and Matsushiro. On the other hand, calcite precipitation accumulated in the inlet in Namikata. In the case of Namikata, the amount of carbon fixation as a solid phase was limited to precipitate because the supersaturated fluid cannot flow into deeper parts of porous media owing to the accumulation of suspended calcite particles occurring around the inlet. In order to store carbonate sustainably, the conditions in the Ogachi and Matsushiro cases are more suitable for mineral trapping than the Namikata case.

CHAPTER 5   DETERMINATION OF INJECTION PARAMETERS

5.1   Introduction

Permeability is the property of porous media allowing the seepage of fluids through interconnected void spaces. If the pore spaces are clogged with deposits, permeability will decrease with the amount of deposits per pore volume. In order to adopt the new findings from previous chapters using simulation, this chapter is devoted to representing an implicit relationship between the amount of fixed carbonates and permeability change in order to provide optimized injection conditions for large amounts of fixation without clogging pore space near the inlet. Therefore, sensitivity analysis for permeability and mineral fixation was performed by changing the hydraulic gradient or the influent Ca concentration of carbonated fluid while comparing to the experimental conditions.

Considering the clogging models on CO_2 sequestration, the real field consists of fractured rocks (e.g. granite) or sedimentary rocks (e.g. sandstone). The following section discusses the influence of temperature and filtration effects on the deposited mass based on the geochemical clogging model proposed in the previous chapter. Hence, the determination of injection parameters was evaluated only in porous media type, not fracture type.

5.2   Evaluation of fixed Ca

Cumulative flow rate of injected carbonate fluid (Q) includes the integral of flow rate (q) over time and can be approximated numerically as a summation of injection

volume per unit time in Eq.(5.1). However, the duration of injection should be divided into sufficiently small increments, as shown in Fig. 5.1.

$$Q = \int q dt \approx \sum (q \Delta t) \tag{5.1}$$

Because the influent concentration was nearly constant, the total amount of Ca in injected fluid is provided by the product of cumulative injection volume from the observed flow rate curves in three cases (Fig. 5.2) as well as the influent Ca concentration (Table 3.3). The particles included in the influent fluid do not always adhere to the surface of porous media. The calculated amount of Ca retained in the column ($M_{i,j}$) can be integrated over the layer consisting of porous media as follows:

$$M_{i,j} = \int_0^L \sigma_{i,j} n_{i,j} A dx \tag{5.2}$$

Where $\sigma_{i,j}$ is the amount of carbonates deposited in the pore volume after the experiments, $n_{i,j}$ is porosity and A is the cross-sectional area of the material perpendicular to the flow direction.

A geochemical clogging model was used to calculate the amount of fixed Ca occupying the initial pore volume in three experimental cases. The calculated amount of deposited Ca for the Matsushiro, Ogachi, and Namikata case corresponds to 36%, 34% and 13% of the initial pore space being occupied by retained Ca respectively.

Fig. 5.3 shows that the Ogachi case at high temperature and the Namikata case at high pH might have contributed to the large calculated amount of deposited Ca. In terms of retention efficiency, a high filtration coefficient correlates with the high ratio of retained Ca to the amount of injected Ca.
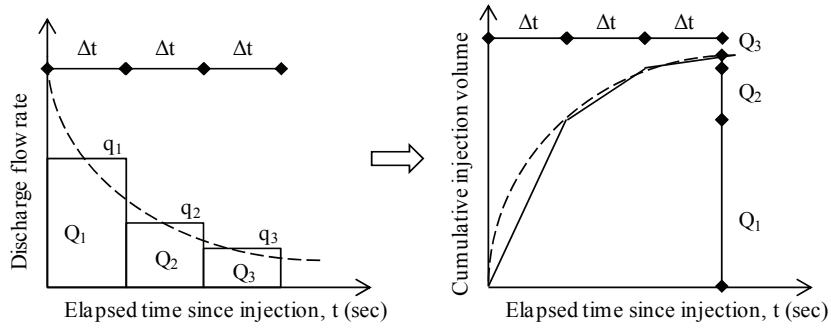
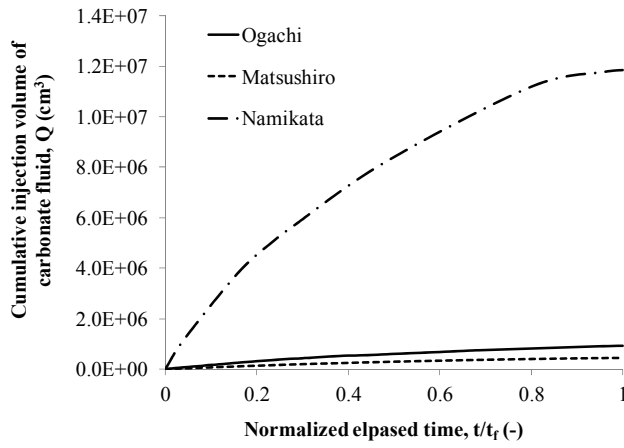Fig. 5.1: Schematic diagram of cumulative injection volume.

Fig. 5.2: Cumulative flow rate of injected fluid in all cases.
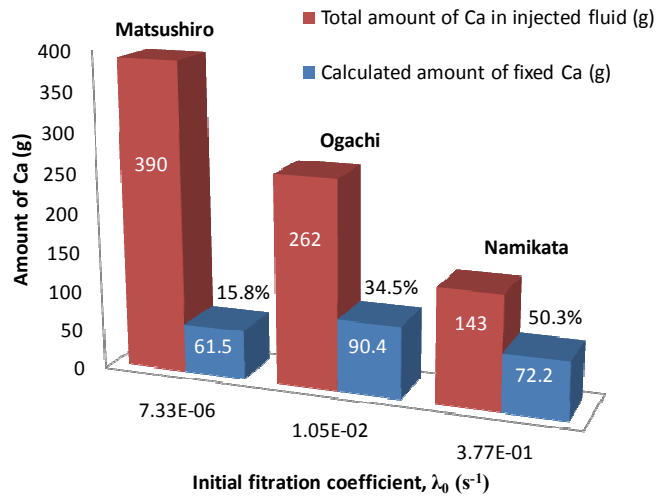

Fig. 5.3: Ratio of Ca fixation with the filtration coefficient.

5.3   Results and discussion

5.3.1   Sensitivity analysis with equivalent permeability

The permeability change curve can provide valuable information about clogging points in terms of when and where decreases in permeability occur. However, due to the distribution of deposits, permeability with respect to elapsed time has different curves depending on the location of porous media in carbonate fluid flow experiments. Thus, equivalent permeability along the section of the column was determined representatively in order to understand when permeability decreases rapidly. A schematic diagram for column experiments is illustrated in Fig. 5.4. This column consists of several layers that have different permeability for flow in the vertical direction due to deposited carbonates. If this stratification is continuous, flow rate is the same for all layers as follows:

$$q_j = q_{1,j} = \cdots = q_{i,j} = \cdots = q_{n,j} \tag{5.3}$$

The subscripts i and j represent the space grid index and the time index and q is the flow rate through the layers 1, 2, $\cdots$, n, respectively. Since Darcy's law is valid in column experiments, the injection volume per unit time at time step j (q_j) has a simple relation as

$$q_j = K_{i,j} iA \tag{5.4}$$
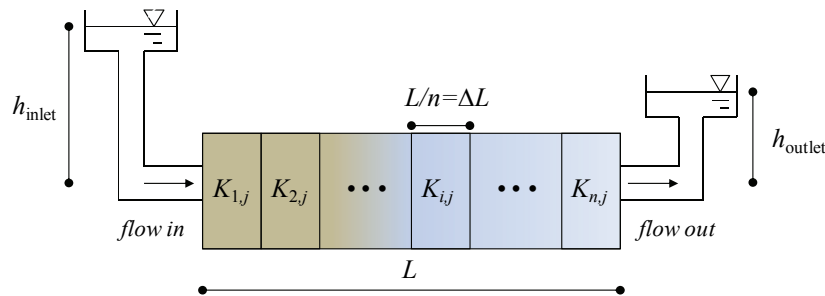

Fig. 5.4: One-dimensional carbonate fluid flow for column experiments.

$$i_{1,j} = \frac{q_j}{K_{1,j}A}$$
$$\vdots$$
$$i_{n,j} = \frac{q_j}{K_{n,j}A}$$
$$i_{eq} = \frac{q_j}{K_{eq,j}A}$$

$$(5.5)$$

where the subscript eq means equivalent.

For flow at right angles to the direction of layers, total head loss (Δh) is the sum of head loss in each layer of Eq.(5.6), which also can be expanded in Eq.(5.7).

$$\Delta h = \Delta h_1 + \Delta h_2 + \cdots + \Delta h_n \tag{5.6}$$

$$i_{eq}L = i_{1,j}\Delta L + i_{2,j}\Delta L + \cdots + i_{n,j}\Delta L \tag{5.7}$$

Combining Eqs.(5.5) and (5.7), the equivalent permeability is a one-dimensional flow that can be calculated in the following equation:

$$K_{eq,j} = \frac{n}{\dfrac{1}{K_{1,j}} + \dfrac{1}{K_{2,j}} + \cdots \dfrac{1}{K_{n,j}}} \tag{5.8}$$

The sensitivity analysis for permeability including the equivalent one, was performed in three column experiments by changing the hydraulic gradient or the initial Ca concentration based on experimental conditions.

High temperature case (Ogachi)

By changing the normalized hydraulic gradient and the influent Ca concentration with the experimental parameters, the normalized equivalent permeability declines with injection time. Fig. 5.5 shows that the normalized equivalent permeability decreases with increasing i/i_0, and converges to about 20% when i/i_0 is greater than 3. In contrast, the increase in C/C_i brings an effect of early mineral trapping, hence, permeability decreases rapidly up to less than 10%, as shown in Fig. 5.6.

High concentration case (Matsushiro)

As shown in Fig. 5.7, the normalized permeability began to decrease rapidly after around $t=80,000$s. The change of i/i_0 results from the acceleration of precipitation rates. Although permeability shows a trend of decline with the increasing hydraulic gradient, the effect of pressure is not influential on permeability. As with similar trends, such as the Ogachi case, increasing C/C_i tends to decrease the normalized equivalent permeability and shorten the time required to less than 10% of the initial flow rate (Fig. 5.8). Therefore, increasing the influent Ca concentration is more advantageous than increasing the hydraulic gradient in order to accelerate the fixation rate.

High pH case (Namikata)

In the three cases shown in Fig. 5.5, Fig. 5.7 and Fig. 5.9, the hydraulic gradient (i/i_0) is the most sensitive to permeability change. The normalized equivalent permeability reaches less than 10% when i/i_0 is more than three. However, the influent concentration (C_i) rather than the hydraulic gradient (i), greatly impacts the permeability change so that clogging will be promoted, as shown in Fig. 5.10.

Fig. 5.5: Sensitivity analysis of the normalized equivalent permeability
with hydraulic gradient for the high temperature case.

Fig. 5.6: Sensitivity analysis of the normalized equivalent permeability
with the influent concentration the high temperature case.

Fig. 5.7: Sensitivity analysis of the normalized equivalent permeability with hydraulic gradient for the high concentration case.

Fig. 5.8: Sensitivity analysis of the normalized equivalent permeability with the influent concentration for the high concentration case.
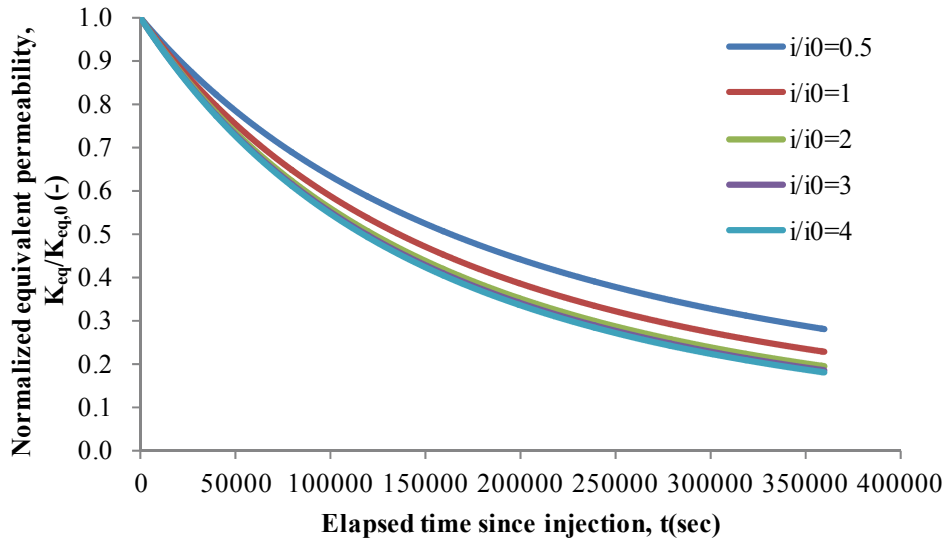
Fig. 5.9: Sensitivity analysis of the normalized equivalent permeability with hydraulic gradient for the pH concentration case.

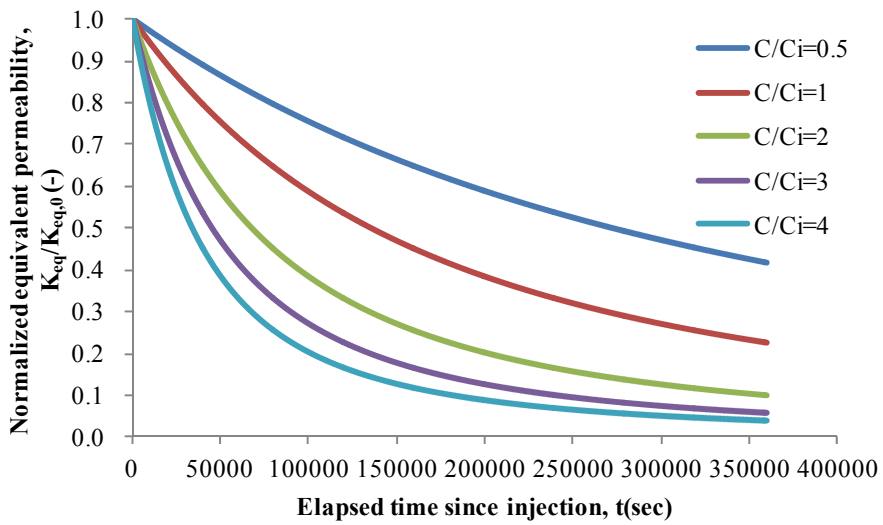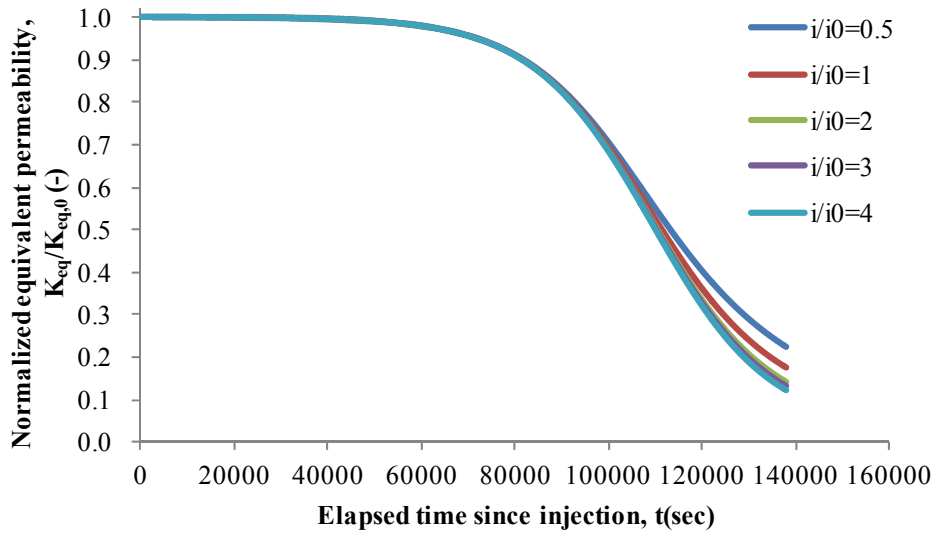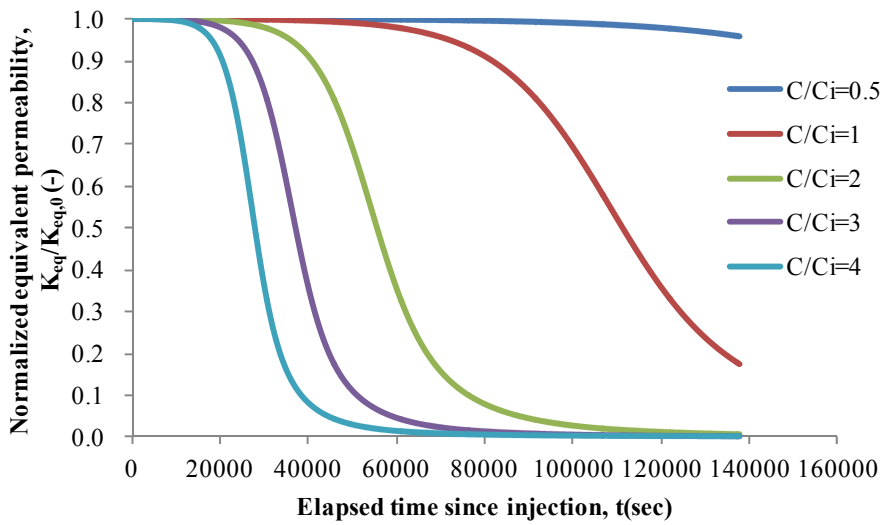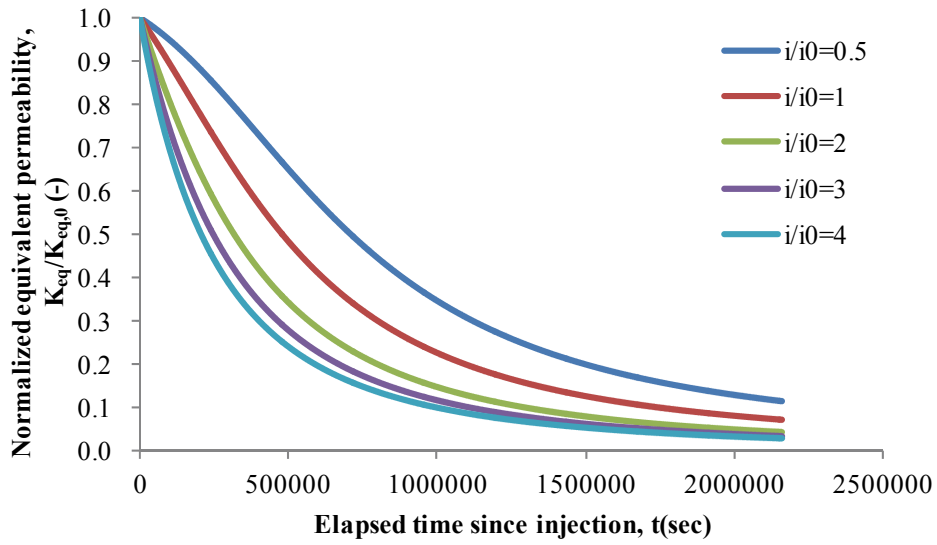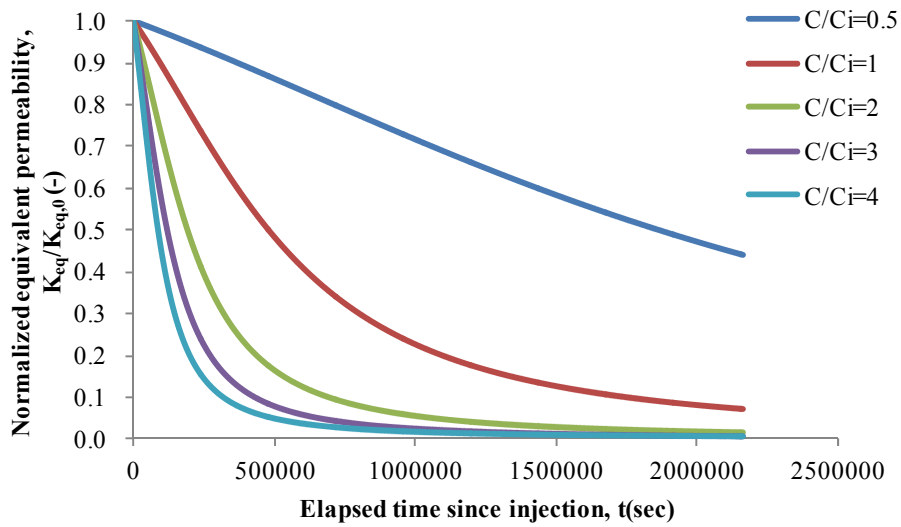Fig. 5.10: Sensitivity analysis of the normalized equivalent permeability with the influent concentration for the high pH case.

5.3.2   Design parameters for maximum fixed amount

Environment-friendlier injection with low costs is needed to minimize the influent concentration of injected chemical substances (C_i) as much as possible. We also have to consider factors for mechanical safety, such as ensuring that the hydraulic gradient (i) is not greater than the pressure of the rock strength. Satisfying these requirements, engineers should try to ascertain achievable conditions to maximize the mineral fixation of CO_2. Therefore, we studied the sensitivity analysis based on laboratory experimental conditions by changing the influent concentration or the hydraulic gradient.

While varying only i/i_0 without changing the other parameters, the fixed amount plotted in Fig. 5.11 converged at $i/i_0 \geq 3$ in the Ogachi and Matsushiro case. For the Namikata case, simulation results above 10 of i/i_0 confirmed that the potential amount of fixed carbonates showed about 3.5 times of one at i_0 enough to locate deposits in the remaining pore volume further from the inlet. The maximum amount of fixed carbonates represented by Fig. 5.12 depends on the filtration coefficient at the threshold of i/i_0.

While controlling only C/C_i while fixing other parameters, the fixed amount results in Fig. 5.13 for the Ogachi, Matsushiro and Namikata cases showed maximums at 1, 2 and 10 of C/C_i. In addition, Fig. 5.14 indicates that the maximum amount of fixed carbonates is temperature dependent because the solubility product of $CaCO_3$ shows lower values at high temperatures. In the case of Namikata at room temperature, the amount of fixed deposits peaked at the same amount in experimental conditions. However, Ogachi and Matsushiro, are available to trap 1.9 and 1.5 times the fixed amount of carbonates in experimental conditions. Therefore, these results suggest that high temperature environments, such as hydrothermal systems or hot spring water is more efficient for mineral trapping in reacting to $CaCO_3$ in porous media.
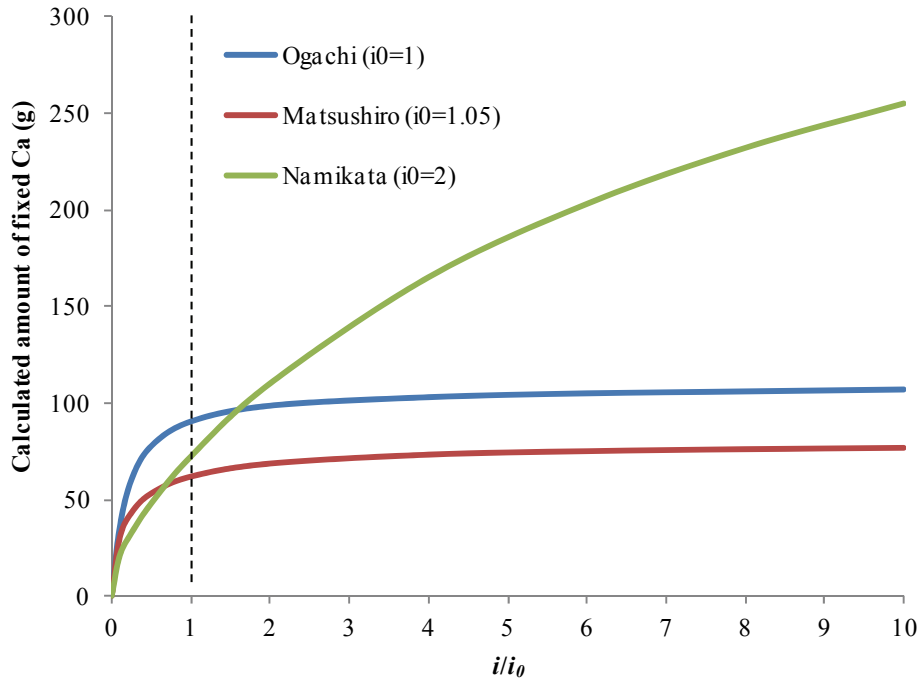
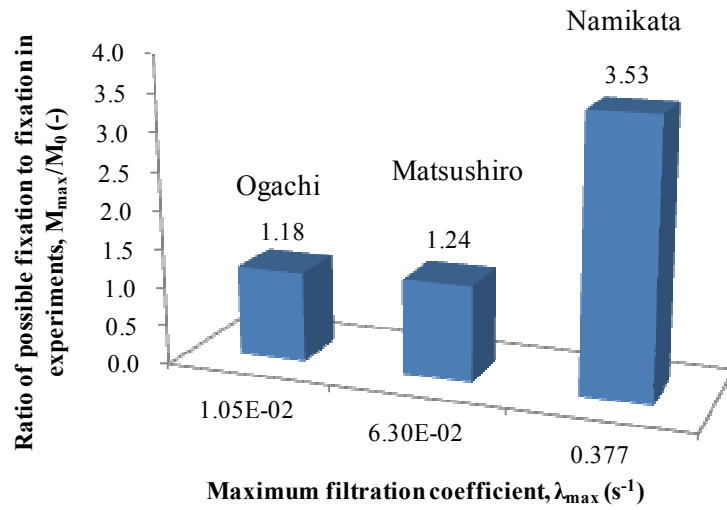Fig. 5.11: Calculated amount of fixed Ca with the ratio of hydraulic gradients.

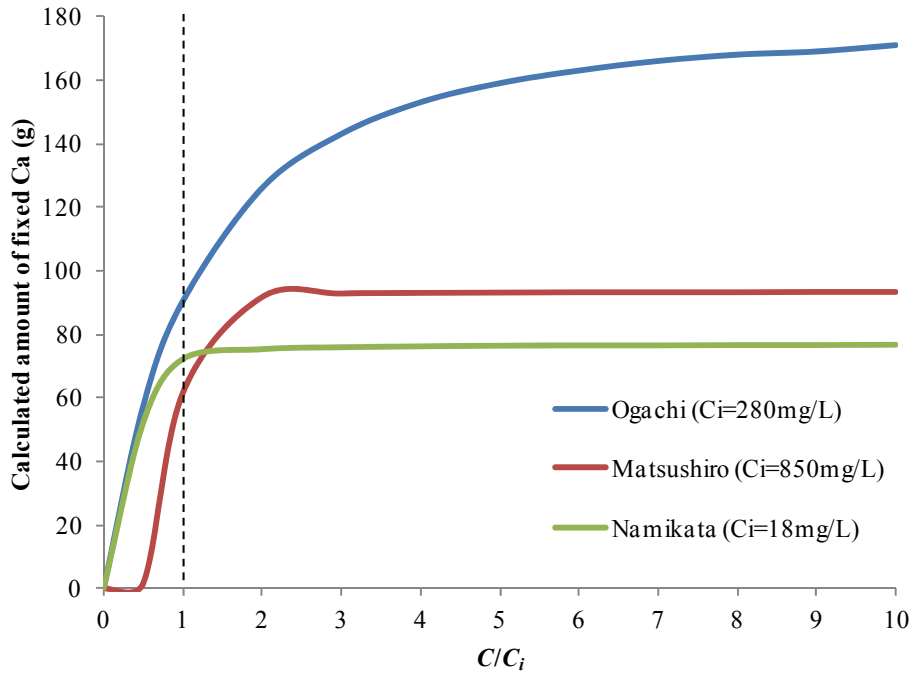Fig. 5.12: Potential amount of fixed Ca with maximum filtration coefficient.

Fig. 5.13: Calculated amount of fixed Ca with the ratio of influent concentration.
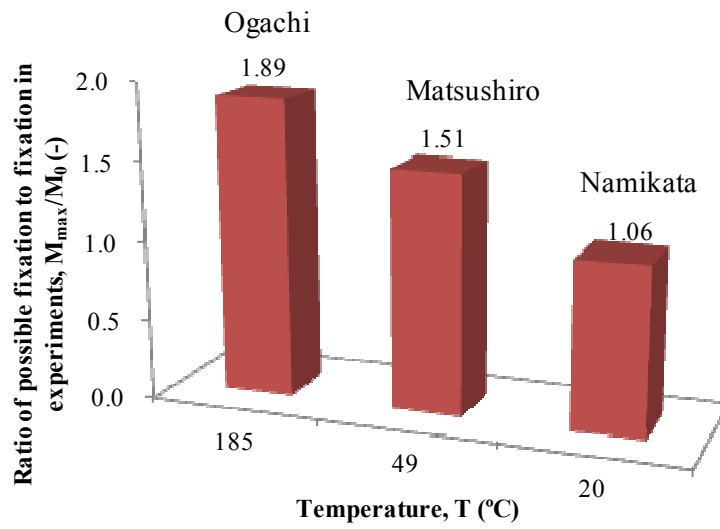

Fig. 5.14: Potential amount of fixed Ca with temperature.

5.3.3   Impact range of reduced permeability

The integrated area between the fixed amount of deposits curves at experimental conditions. The threshold of i/i_0 or C/C_i correlates with the potential amount of fixed carbonates. The simple method of using the integrated area can distinguish intuitively the more sensitive factor which causes a sharp drop of permeability. As a result of permeability with respect to the location of the column, it is possible to predict the influential range in which carbonate deposits migrate from the injection point.

The comparison of Fig. 5.15 and Fig. 5.16 for the high temperature case and Fig. 5.17 and Fig. 5.18 for the high concentration case indicates that controlling the concentration rather than the hydraulic gradient is likely to decrease permeability under relatively high temperatures. The higher the concentration of carbonates rises up, the higher the probability of the clogging near the inlet, as shown in Fig. 5.16 and Fig. 5.18. In order to inhibit this problem, the higher hydraulic gradient represented by Fig. 5.15 and Fig. 5.17 can maintain permeability uniformly, just like the one at the inlet.

In contrast, in the high pH case, for example in the Namikata case, the hydraulic gradient presented by Fig. 5.19 is more sensitive than the concentration presented by Fig. 5.20 in order to maximize the amount of mineral trapping. As shown in Fig. 5.20, the higher fluid velocity provides further migration of deposited carbonates by increasing the hydraulic gradient so that the impact range of reduced permeability expands. The concentration does not affect permeability change because of the maximum deposits at the concentration, C_i.

Fig. 5.15: Sensitivity analysis of the normalized permeability distribution with hydraulic gradient for the high temperature case.

Fig. 5.16: Sensitivity analysis of the normalized permeability distribution with the influent concentration for the high temperature case.

Fig. 5.17: Sensitivity analysis of the normalized permeability distribution
with hydraulic gradient for the high concentration case.
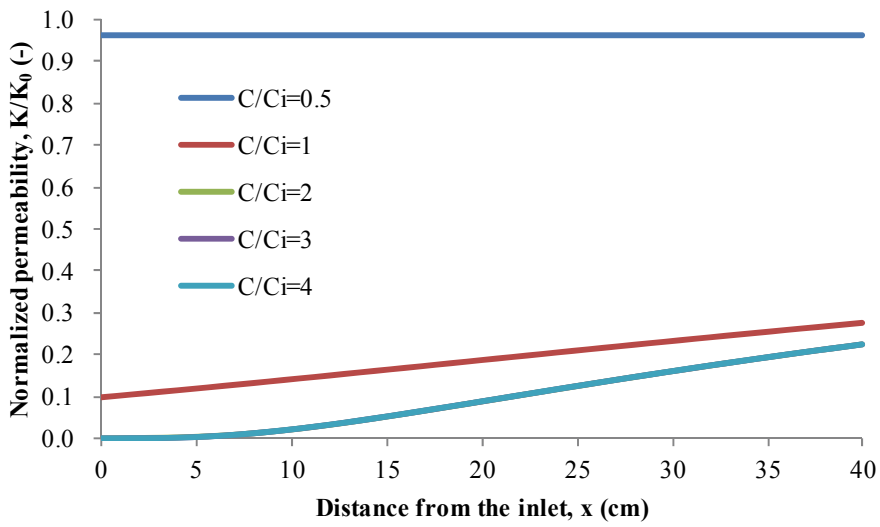
Fig. 5.18: Sensitivity analysis of the normalized permeability distribution
with the influent concentration for the high concentration case.
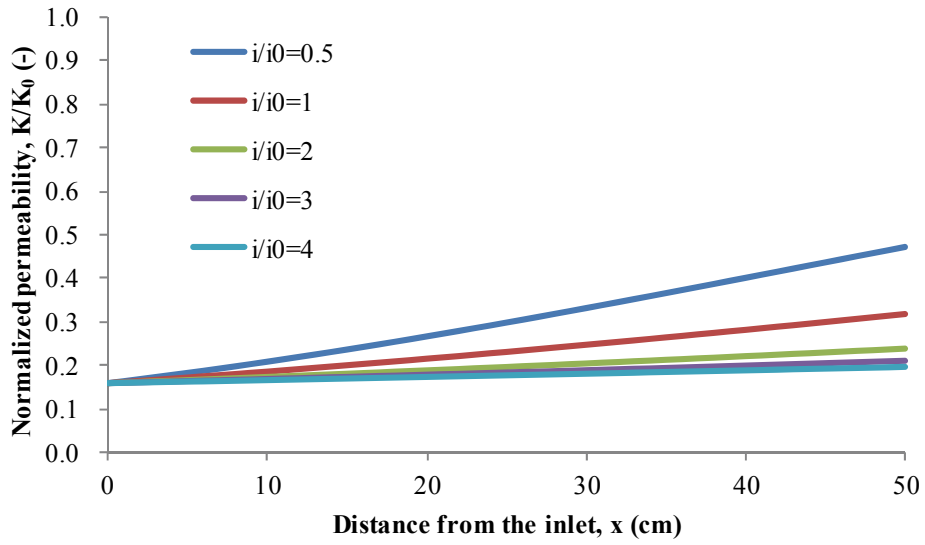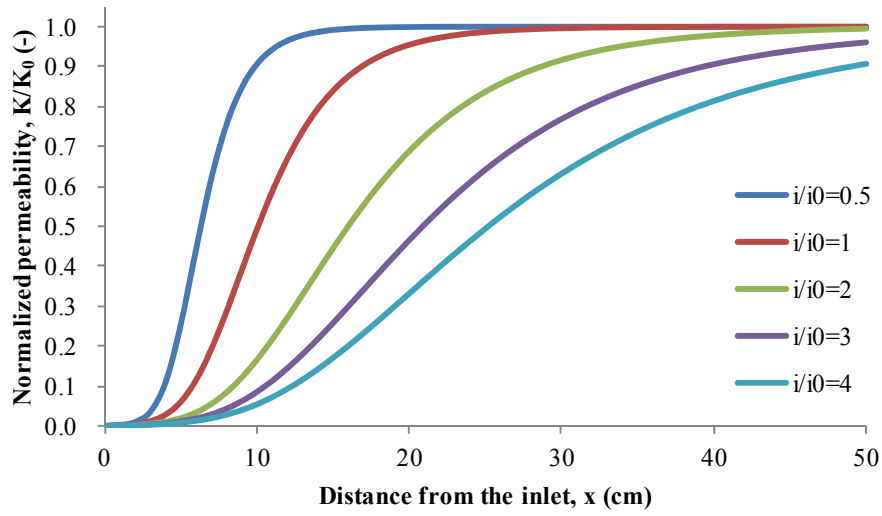
Fig. 5.19: Sensitivity analysis of the normalized permeability distribution
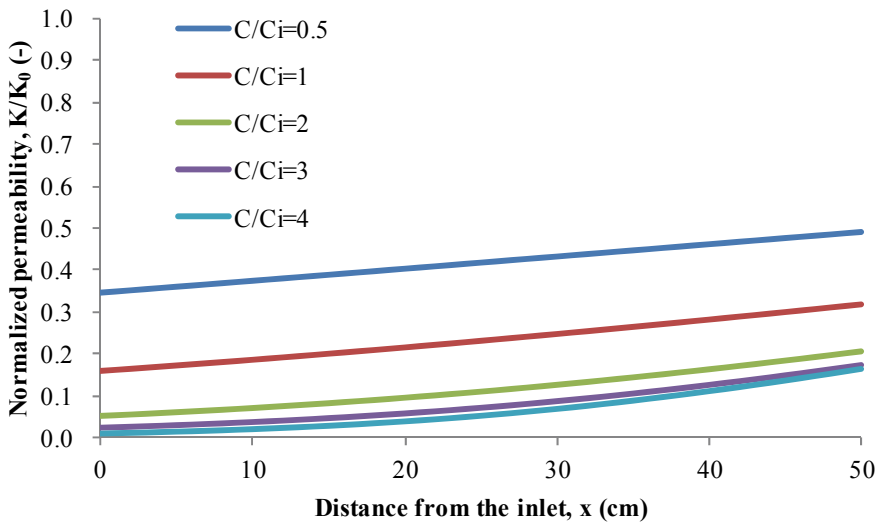with hydraulic gradient for the high pH case.
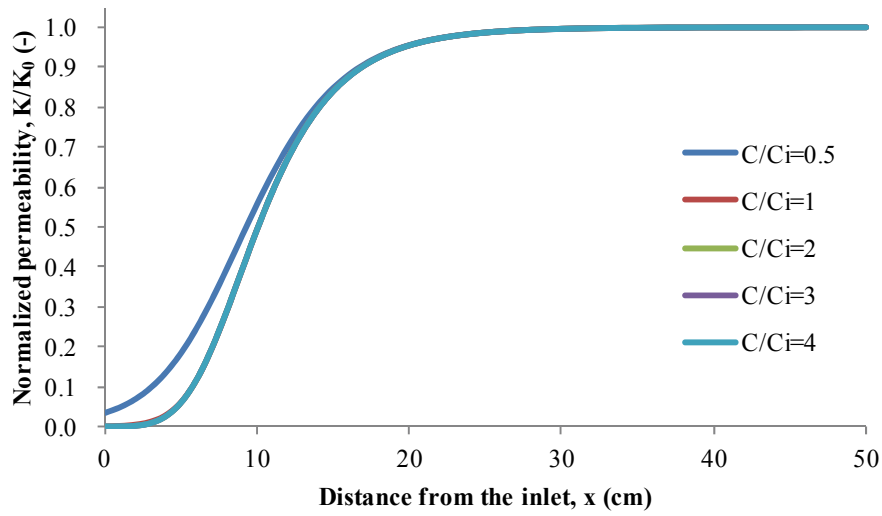
Fig. 5.20: Sensitivity analysis of the normalized permeability distribution
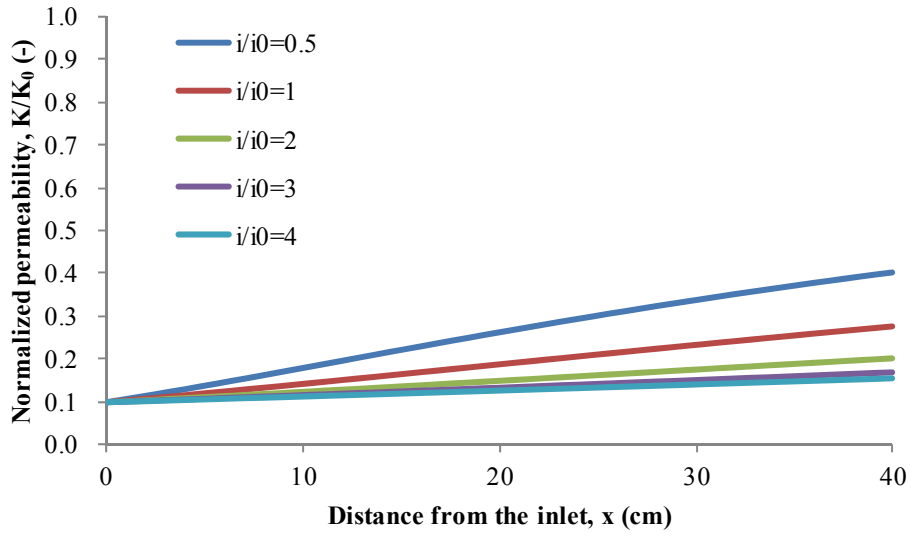with the influent concentration for the high pH case.

5.4   Conclusions

In this chapter, various results simulated by the geochemical clogging model provide best conditions for mineral trapping, particularly regarding how to migrate mineral particles further from the injection part and store as much as possible in the pore space without clogging. Thus, the sensitivity analysis about permeability and the amount of fixed carbonates provides helpful information by illustrating the difference between the experimental conditions of the hydraulic gradient and influential concentration.

The control of the influent concentration of carbonates is more critical than the hydraulic gradient for maximizing mineral trapping at high temperatures, such as hydrothermal conditions. In the cases of Ogachi and Matsushiro, the possible amount of fixed carbonates is 1.9 and 1.5 times higher in the experimental conditions, respectively.

In contrast, at relatively low temperatures and high pH, for example in the Namikata case, the hydraulic gradient is more sensitive than the change of concentration for mineralization. Simulation results provided 3.5 times the amount of fixed carbonates in experimental conditions when i is equal to 10 times of i_0. The higher fluid velocity results in the further migration of the deposited particles so that influential range is enlarged by the decrease of permeability distribution.

CHAPTER 6   CONCLUDING REMARKS

In this thesis, a newly-developed geochemical clogging model aims to provide predictions of when and where carbonate deposits might be found through reservoirs during CO_2 sequestration. A series of flow experiments through porous media using a supersaturated carbonate fluid also was performed in order to observe the flow rate curves. Meanwhile, to evaluate precipitation rates and permeability change in the formation, calculated flow rates based on the proposed geochemical clogging model were compared with the experimentally observed data. From low to high temperatures, various cases were studied to understand how temperature and pH can affect precipitation rates of carbonates. The main conclusions drawn from the present study are summarized as follows.

In chapter 2, a series of studies were conducted on CO_2 geological sequestration and scale problems under the hydrothermal conditions. We focused on a numerical simulation about mineral precipitation and zero emission systems for geothermal power plants.

In chapter 3, the purpose of flow experiments was to clarify the relationship between the saturation index (S.I.) of carbonates and precipitation rates in rock formations. S.I. generally depends on temperature and pH, so supersaturated fluid with carbonates (S.I.=1.1~1.8) flowed into in-situ rock formation or porous media when maintaining high temperatures or pH. Column experiments at Ogachi and Matsushiro were performed at high (185ºC) and middle (49ºC) average temperatures. In the Namikata case, the pH of the groundwater in the tunnel showed alkaline enough to precipitate carbonates even though the fluid indicates a lower concentration of Ca^{2+} and

HCO_3^-. In previous research, Kuroda (2009) reported that precipitation rates are associated to the product of S.I. and CO_2 concentration (S.I. x [CO_2]) rather than S.I. value. The high S.I. and the high concentration of chemical reactants (Ca and CO_2) directly contribute to the crystal growth of carbonate mineral. As such, the very high concentration of reactants made it possible to form deposits in spite of the relatively low S.I. condition. The large order in S.I. x [CO_2], such as Matsushiro, Ogachi, and Namikata aligned well with the order of required clogging time, which defined as duration by when the flow rate declined up to about 10 % of the initial flow rate.

In chapter 4, a step-wised numerical calculation method was developed in both physical and geochemical contexts in order to predict when and where permeability change would occur. A physical clogging model provided permeability change only with respect to injection time. However, a geochemical clogging model was extended to provide predictions of when and where carbonate deposits might be found through reservoirs during carbonate fluid injection. We found that the ratio of the filtration coefficient to fluid flow velocity (λ/u) was a key parameter in understanding the distribution of carbonate precipitation. The smaller the λ/u, the more uniform the amount of deposits, as shown in the cases of Ogachi and Matsushiro. In contrast, the amount of carbonates decreased exponentially with distance from the inlet in Namikata due to a relatively larger λ/u than in other cases. Therefore, the mineral fixation will have difficulties penetrating into deeper parts of porous media because suspended carbonate particles were concentrated near the inlet. In this respect, for mineral trapping, the conditions in the Ogachi and Matsushiro cases are better than the Namikata case for storing carbonate sustainably. Even if the high pH condition might be inappropriate for CO_2 sequestration due to scale problems around the borehole, the carbonate mechanism

at the low temperature is worth comparing with at the high temperature and the neutral pH.

In chapter 5, sensitivity analysis for permeability and the amount of fixed carbonates was suggested to determine the design parameters for the injection of carbonate fluid how far and how much the mineral particles would be retained in the column without clogging pore spaces. Analysis results showed that a decrease of permeability created a noticeable difference between change of the hydraulic gradient and the influent Ca concentration.

At high temperatures, such as the cases of Ogachi and Matsushiro, the effect of the influent concentration is more critical than the hydraulic gradient because the maximum amount of fixed carbonates will increase by a factor of 1.9 and 1.5 respectively, compared to the one in the experimental conditions.

In contrast, at relatively low temperatures and high pH instances, such as the Namikata case, higher hydraulic gradients create an advantage for mineralization without clogging than higher concentrations. Simulation results show that 3.5 times the amount of carbonates in the experimental conditions are available at the high hydraulic gradient (i/i_0=10). In other words, the higher fluid velocities result in further migration of the deposited particles, while extending the influential range determined by decreased permeability.

However, all the numerical calculations presented in this thesis are one-dimensional and at laboratory scale. For the successful design of various geomechanical and geochemical engineering projects, such as geothermal energy exploration and CO_2 sequestration in hydrocarbon reservoirs, more detailed analysis is required using not only one-dimensional simulations but also two or three-dimensional and fracture type simulations. These possibilities will be explored in future work.

References

Arnórsson, S., Sigurdsson, S., Svarvarsson, H., 1982. The chemistry of geothermal waters in Iceland. I. Calculation of aqueous speciation from 0° to 370°C. Geochim. Cosmochim. Acta. 46, 1513-1532.

Audigane, P., Gaus, I., Pruess, K., Xu, T., 2006. A long term 2D vertical modelling study of CO_2 storage at Sleipner (North Sea) using TOUGHREACT. Proceedings of TOUGH Symposium.

Bachu, S., Bonijoly, D., Bradshaw, J., Burruss, R., Holloway, S., Christensen, N.P., Mathiassen, O.M., 2007. CO_2 storage capacity estimation: methodology and gaps. Int. J. Greenhouse Gas Control 1, 430–443.

Bickle, M., Chadwick, A., Huppert, H.H., Hallworth M., Lyle S., 2007. Modelling carbon dioxide accumulation at Sleipner: implications for underground carbon storage. Earth Planet. Sci. Lett. 255, 164-176.

Brown, C. A., Comoton, R. G., Narramore, C. A., 1993. The kinetics of calcite dissolution /precipitation. J. Coll. Inter. Sci. 160, 372-379.

Carrier, W.D., 2003. Goodbye, Hazen; Hello, Kozeny-Carman. J. Geotech. Geoenvir. Engrg., ASCE, 129, 11, 1054-1056.

Chiba, H., 1991. Attainment of solution and gas equilibrium in Japanese geothermal systems. Geochem. J. 25, 335-355.

Gales, C., Shane, H., 1905. About a case of kaolinitisation in granite by a cold CO_2 bearingwater. Zenlt. Geol. Min. Palisant. 427-467.

Gruesbeck, C., Collins, R.E., 1982. Entrainment and deposition of fine particles in porous media. Soc. Petro. Eng. J. 22, 6, 847-856.

Gunter, W.D., Bird, G.W., 1988. CO_2 production in tar sand reservoirs under in situ steam temperatures: Reactive calcite dissolution, Chem. Geol. 70, 301-311.

Hvorslev, M.J., 1951. Time Lag and Soil Permeability in Ground-Water Observations, Bull. No. 36, Waterways Exper. Sta. Corps of Engrs, U.S. Army, Vicksburg, Mississippi, 1-50.

Irabien, A., Viguri, J., Ortiz, I., 1990. Thermal dehydration of calcium hydroxide. 1. Kinetic Model and Parameters. Ind. Eng. Chem. Res. 29, 1599-1606.

IEA, 2009. Technology Road map: Carbon Capture and Storage. 1-7.

IPCC, 2005. Underground geological storage in IPCC Special Report on Carbon Dioxide Capture and Storage. 195-276.

Ito, H., Kitano, K., 1999. Estimation of fracture structure in reservoir for Hot Dry Rock geothermal power: fracture orientation in the Ogachi reservoir estimated by bore hole televiewer. CRIEPI Report. U98054, 1-21.

Ito, H., Kaieda, H., Suenaga, H., Kubota, K., 2011. Field experiments on CO_2 sequestration at Ogachi Hot Dry Rock site (part2) - application of calcite precipitation and permeability and permeability tests and evaluation for their improvements -. CRIEPI Report. N10051, 1-20.

Itoi, R., Fukuda, M., Jinno, K., Yokoyama, T., 1987. Decrease in reservoir permeability due to deposition of silica dissolved in geothermal injection water - numerical simulation in one dimensional flow system -. J. Geotherm. Res. Soc. Japan. 9, 4,

285-306.

Itoi, R., Fukuda, M., Jinno, K., Yokoyama, T., 1987. Decrease in reservoir permeability due to deposition of silica dissolved in geothermal injection water - numerical simulation in one dimensional flow system -. J. Geotherm. Res. Soc. Japan. 9, 4, 285-306.

Ives, K.J., 1975. Mathematical models of deep bed filtration. NATO adv. study inst.ser. E. Applied Sciences. 2, 203-224.

Jonasson, R.G., Rispler, K., Wiwchar, B., Gunter, W.D., 1996. Effect of phosphonate inhibitors on calcite nucleation kinetics as a function of temperature using light scattering in an autoclave. Chem. Geol. 132, 215-225.

Kato, H., Kamei, J., Kitao K., 2000. Fluid flow - precipitation model of anhydrite scale in wellbore -case study of the Sumikawa production well -. SC-1. J. Geotherm. Res. Soc. Japan. 22, 3, 171-185.

Kaieda, H., Ito, H., Kiho, K., Suzuki, K., Suenaga, H., Shin, K., 2005. Review of the Ogachi HDR Project in Japan. Proceedings of World Geothermal Congress. 1601.

Kaieda, H., Kubota, K., Ito, H., Ohsumi, T., Wakahama, H., Mito, S., 2009. Field experiments for studying on CO_2 sequestration in mineral at Ogachi HDR site. CRIEPI Report. N08051, 1-22.

Kim, J.S., Lee I.M., Jang J.H., Choi H.S., 2009. Groutability of cement-based grout with consideration of viscosity and filtration phenomenon. Int. J. Numer. Anal. Geomech. 33, 1771-1797.

Kim, J. W., Matsuoka, T., Xue, Z., 2011. Monitoring and detecting CO_2 injected into water-saturated sandstone with joint seismic and resistivity measurements. Co-published paper -Exploration Geophysics, 42, 1–10; Butsuri-Tansa, 64, 1–10; Mulli-Tamsa, 14, 1–10.

Kitano, Y., Kanamori, N., Tokuyama, A., 1969. Effects of organic matter on solubilities and crystal form of carbonates. Am. Zoologist. 9, 681-688.

Kuroda, Y., Yamada, Y., Ueda, A., Matsuoka, T., Yamada, N., 2009. Experimental research of plagioclase (rock)-gas-water interaction at hydrothermal conditions for CO_2 mineralization. Jap. Mag. Mineral. Petro. Sci. 38, 111-121.

Lee, D.S., Elsworth, D., Yasuhara, H., Weaver, J.D., Rickman, R., 2010. Experiment and modeling to evaluate the effects of proppant-pack diagenesis on fracture treatments. J. Pet. Sci. Eng. 74, 67-76.

Lee, Y.J., Morse, J.W., Wiltschko D.V., 1996. An experimentally verified model for calcite precipitation in veins. Chem. Geol. 130, 203-215.

Lee, Y.J., Morse, J.W., 1999. Calcite precipitation in synthetic veins: implications for the time and fluid volume necessary for vein filling. Chem. Geol. 156, 151-170.

McDowell-Boyer, L.M., Hunt, J.R., Sitar, N., 1986. Particle transport through porous media. Water Resour. Res. 13, 1901-1921.

Meyer, H.J., 1984. The influence of impurities on the growth rate of calcite. J. Crystal Growth. 66, 639-646.

Mito, S., Xue, Z., Ohsumi, T., 2008. Case study of geochemical reactions at Nagaoka CO_2 injection site, Japan. Int. J. Greenhouse Gas Cont. 2. 309-318.

Morse, J.W., Mackenzie, F.T., 1993. Geochemical constraints on $CaCO_3$ transport in subsurface sedimentary environments. Chem. Geol. 105, 181-196.

Muraoka, H., 2009. Carbon dioxide emissions from geothermal power plants in Japan and their future trends. Proceedings of Annual Meeting Geothermal Research Society of Japan. B02.

Oriyama, J., Iwahara, T., Takayama, N., 2007. Energy Stockpiling and Underground Storage. The Japanese Geotechnical Society. 55, 4, 35-38.

Ozawa, A., Ueda, A., Nishimura, Y., Sato, H., Tsukamoto, K., 2006. Geochemical monitoring of calcite precipitation and dissolution in Ca rich ground waters with a newly developed interferometer. Proceedings of 19th General Meeting of the International Mineralogical Association. 168.

Parkhurst, D.L., Appelo, C.A.J., 1999. Users Guide to PHREEQC (Version 2) - A computer program for speciation, batch-reaction, one-dimensional transport, and inverse geo-chemical calculations. Water-Resources Investigation Report, U.S. Dep. Int., U.S. Geol. Surv. 40-48.

Palandri, J., Kharaka, Y.K., 2004. A compilation of rate parameters of water‑mineral interaction kinetics for application to geochemical modeling. US Geol. Surv. Open File Report 2004-1068. 1-64.

Reddi, L.N., Bonala, M.V.S., 1997. Analytical solution for fine particle accumulation in soil filters. J. Geotech. Geoenvir. Engrg., ASCE, 123, 12, 1143–1152.

Reddi, L.N., Xiao, M., Hajra, M.G., Lee, I.M., 2000. Permeability reduction of soil filters due to physical clogging. J. Geotech. Geoenvir. Engrg., ASCE, 126, 3, 236–246.

Reddi, L.N., Xiao, M., Hajra, M.G., Lee, I.M., 2005. Physical clogging of soil filters under constant flow rate versus constant head. Can. Geotech. J. 42, 804–811.

RITE, 2008. Development of a technology for CO_2 fixation and sequestration using serpentinite rock mass. Annual report. 1-184.

Shikazono, N., Harada, H., Ikeda, N., Kashiwagi, H., 2009. Dissolution of basaltic rocks and its application to understand sequestration of CO_2 -Estimate of mineral trapping by dissolution-precipitation simulation-. J. Miner. Soc. Jap. 38, 149-160.

Shiraki, R., Brantley, S.L., 1995. Kinetics of near-equilibrium calcite precipitation at 100 °C: An evaluation of elementary reaction-based and affinity-based rate laws. Geochim. Cosmochim. Acta. 59, 8, 1457-1471.

Sorai, M., Ohsumi, T., Ishikawa, M., Tsukamoto, K., 2007. Feldspar dissolution rates measured using phase-shift interferometry: Implications to CO_2 underground sequestration. Appl. Geochem. 22, 2795-2809.

Suto, Y., Liu, L., Yamasaki, N., Hashida, T., 2007. Initial behavior of granite in response to injection of CO_2-saturated fluid. Appl. Geochem. 22, 2795-2809.

Teng, H.H., Dove, P.M., Yoreo, J.J., 2000. Kinetics of calcite growth: Surface processes and relationships to macroscopic rate laws. Geochim. Cosmochim. Acta. 64,13, 2255-2266.

Ueda, A., Kato, K., Ohsumi, T., Yajima, T., Ito, H., Kaieda, H., Metcalf, R., Takase, H., 2005. Experimental studies of CO_2-rock interaction at elevated temperatures under hydrothermal conditions. Geochem. J. 39, 417-425.

Witherspoon, P.A., Wang, J.S.Y., Iwai, K., Gale, J.E., 1979. Validity of cubic law for fluid flow in a deformable rock fracture. Water Resour. Res. 16, 6, 1016-1024.

Xu, T., Ontoy Y., Molling, P., Spycher N., Parini M., Pruess K., 2004a. Reactive transport modeling of injection well scaling and acidizing at Tiwi field, Phillippines. Geothermics. 33, 477-491.

Xu, T., Apps, J.A., Pruess, K., 2004b. Numerical simulation of CO_2 disposal by mineral trapping in deep aquifers. Appl. Geochem. 19, 917-936.

Xu, T., Sonnenthal, E.L., Spycher, N., Pruess, K., 2006. TOURGHREACT: a simulation program for non-isothermal multiphase reactive geochemical transport in variably saturated geologic media. Comput. Geosci. 32, 145–165.

Yoo, S.Y., Kuroda, Y., Mito, Y., Ueda, A., Matsuoka, T., 2011. Physical clogging model using stick rate of calcite on CO_2 mineral trapping. Harmonising Rock Engineering and the Environment, Proceedings of the 12th Congress of the International Society for Rock Mechanics, 1385-1388.

Yoo, S.Y., Ueda, A., Mito, Y., Matsuoka, T., 2012. Estimation of carbonate mineral deposition rates using column tests on CO_2 sequestration at high temperatures. J. Soc. Mater. Sci., Japan. 61, 3, 253-258.

Yoo, S.Y., Kuroda, Y., Mito, Y., Matsuoka, T., Nakagawa, M., Ozawa, A., Sugiyama, K., Ueda, A., 2012. A geochemical clogging model with carbonate precipitation rates under hydrothermal conditions. Appl. Geochem., in press.

Yoo, S.Y., Mito, Y., Ueda, A., Matsuoka, T., 2012. Geochemical clogging in fracture and porous rock for CO_2 mineral trapping, Proceedings of the 11th International

Conference on Greenhouse Gas Control Technologies (GHGT-11), accepted.

Zhang, Y., Dawe, R.A., 2000. Influence of Mg^{2+} on the kinetics of calcite precipitation and calcite crystal morphology. Chem. Geol. 163, 129–138.